Hexagonal Ferrite $MFe_{12}O_{19}$ (M=Sr, Ba, Cu, Ni, Pb) Based Photocatalysts: Photoluminescence, Photocatalysis and Applications

Shifa Wang[1,2,*], Xinmiao Yu[1,2], Huajing Gao[1,2] and Xiangyu Chen[1,2]

[1]*School of Electronic and Information Engineering, Chongqing Three Gorges University, Chongqing, Wanzhou, 404000, China*

[2]*Chongqing Key Laboratory of Geological Environment Monitoring and Disaster Early-warning in Three Gorges Reservoir Area, Chongqing Three Gorges University, Chongqing, Wanzhou, 404000, China*

Abstract: Hexagonal ferrite ($MFe_{12}O_{19}$, M=Sr, Ba, Cu, Ni, Pb) is a kind of semiconductor material with excellent performance and an important magnetic material, with high chemical and thermal stability, low cost, simple preparation process, excellent optical, magnetic, wave-absorbing, dielectric, photoluminescence properties and catalytic activities have been widely used in broadcast communication, information storage, aerospace, automatic control, catalytic synthesis, medicine and biology and many other fields. This paper focuses on the application of $MFe_{12}O_{19}$-based ferrite in the field of photocatalysis, and further discusses the effect of preparation method on the photocatalytic activity of $MFe_{12}O_{19}$-based photocatalysts. The application of $MFe_{12}O_{19}$-based photocatalysts in the degradation of dyes, drugs and persistent organic pollutants (POPs) was deeply revealed, and the photocatalytic mechanisms of single-phase $MFe_{12}O_{19}$, ion-doped $MFe_{12}O_{19}$ and $MFe_{12}O_{19}$-based composite photocatalysts were also explored. The relationship between photocatalytic activity and photoluminescence properties of $MFe_{12}O_{19}$-based photocatalysts have also been investigated. This review points out the direction for further research on the application of $MFe_{12}O_{19}$-based photocatalysts in the field of photocatalysis.

Keywords: Hexagonal ferrite, Photocatalytic activity, Photocatalytic mechanism, Photoluminescence properties, Photocatalysts.

1. INTRODUCTION

The great development of the world economy is the development at the expense of the environment, which has been widely concerned by all countries. [1-4] The clothes people wear in daily life, drugs, textiles, paper will use a large number of dyes, antibiotics and other persistent organic pollutants (POPs), these pollutants directly discharged into the environment, will cause fatal harm to the environment, thus affecting human production and life. [5-8] Therefore, the degradation of dyes, drugs and POPs at source will greatly reduce their harm to the environment. The common practice of scientific researchers is to select appropriate photocatalysts for the photocatalytic degradation of dyes, drugs and POPs by reasonable use of sunlight, and unprecedented progress has been made. [9-18] In spite of this, photocatalyst cannot be recovered in water, which will cause secondary pollution to water body.

Recently, $MFe_{12}O_{19}$ (M=Sr, Ba, Cu, Ni, Pb), as a class of strong magnetic material with high photocatalytic activity, has entered the attention of researchers engaged in photocatalytic research. [19-21] The magnetic field is used to recover the photocatalyst, which greatly reduces the secondary pollution caused by the photocatalyst to water. [22-25] Figure **1**(**a**) shows the crystal structure of $MFe_{12}O_{19}$ photocatalysts. The unit cell of $MFe_{12}O_{19}$ is composed mainly of two building blocks of ‘S’ block $(Fe_6O_8)^{2+}$ and ‘R’ block $(MFe_6O_{11})^{2+}$ has a spinel unit cell and hexagonal closed packing of oxygen ions and M ions, respectively. [26] Figure **1**(**b**) shows the related energy level diagram of $MFe_{12}O_{19}$ photocatalysts. Conduction band potential (E_{CB}) and valence band potential (E_{VB}) of $MFe_{12}O_{19}$ can be calculated by equations (1) and (2).

$$E_{CB} = X - E^{e} - 0.5E_g \tag{1}$$

$$E_{VB} = E_{CB} + E_g \tag{2}$$

Where E^e=4.5 eV, Eg is the optical band gap value of $MFe_{12}O_{19}$. X is the absolute electronegativity of $MFe_{12}O_{19}$. According to formula (3), $X(MFe_{12}O_{19})$ can be obtained.

$$X(MFe_{12}O_{19}) = \sqrt[32]{X(M)X(Fe)^{12}X(O)^{19}} \tag{3}$$

Based on the above formula, the E_{CB} and E_{VB} of $MFe_{12}O_{19}$ photocatalysts are given in Table **1**. With the

*Address correspondence to this author at the School of Electronic and Information Engineering, Chongqing Three Gorges University, Chongqing, Wanzhou, 404000, China; Tel: +86 023 -58106025;
E-mail: wangshifa2006@yeah.net

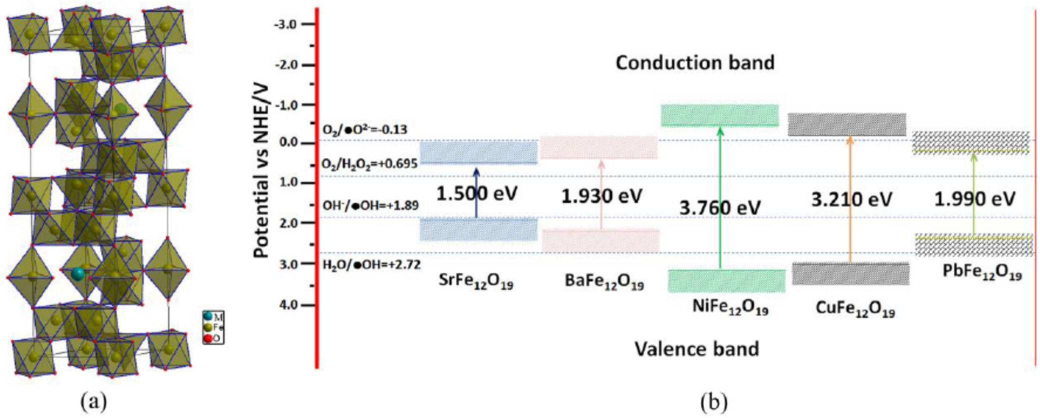

Figure 1: (**a**) Crystal structure and (**b**) the related energy level diagram of $MFe_{12}O_{19}$ photocatalysts.

Table 1: The E_{CB} and E_{VB} of $MFe_{12}O_{19}$ Photocatalysts

Samples	Eg (eV)	X (V)	E_{CB} (V)	E_{VB} (V)	References
$SrFe_{12}O_{19}$	1.500	5.735	0.485	1.985	[27]
$BaFe_{12}O_{19}$	1.930	5.768	0.303	2.233	[28]
$NiFe_{12}O_{19}$	3.760	5.878	-0.502	3.258	[20]
$CuFe_{12}O_{19}$	3.210	5.882	-0.233	2.987	[29]
$PbFe_{12}O_{19}$	1.990	5.856	0.361	2.351	[30]

difference of M ions, the optical band gap of $MFe_{12}O_{19}$ is different, which leads to the difference of conduction band potential and valence band potential, and thus affects the photocatalytic activity of $MFe_{12}O_{19}$. [20, 27-30] Therefore, the design of $MFe_{12}O_{19}$-based photocatalysts for pollutant degradation can be based on the above theory.

Based on the band arrangement theory, a variety of $MFe_{12}O_{19}$-based photocatalysts have been designed to degrade pollutants. [31] In order to promote the degradation of pollutants by $MFe_{12}O_{19}$, Valero-Luna *et al*. [32] enhanced the visible photocatalytic activity of $BaFe_{12}O_{19}$ by adding H_2O_2 to methyl blue dye solution. To reduce the optical bandgap value of $MFe_{12}O_{19}$, ion doping $MFe_{12}O_{19}$ was used to preserve its strong magnetic properties and enhance the photocatalytic activity of the system. [33] Due to the limitation of synthesis methods, most researchers still focus on the construction of heterojunction. [34-42] Based on different synthesis methods of $MFe_{12}O_{19}$-based photocatalysts to construct a recyclable magnetic photocatalyst with high photocatalytic activity, this paper studied the application of $MFe_{12}O_{19}$-based photocatalysts in the degradation of dyes, drugs and POPs, and then summarized the photocatalytic mechanism of different $MFe_{12}O_{19}$-based photocatalysts. Meanwhile, the internal mechanism of photoluminescence and photocatalysis of $MFe_{12}O_{19}$-based photocatalyst is also deeply understood. With the development of science and technology, $MFe_{12}O_{19}$-based photocatalysts are developing towards diversification and optimized performance, with a view to industrial application in the near future.

2. SYNTHESIS OF $MFE_{12}O_{19}$ (M=SR, BA, CU, NI, PB) BASED PHOTOCATALYSTS

Although $MFe_{12}O_{19}$ photocatalyst has high magnetic properties, the metal salt used for synthesis is weak in magnetically, so it is suitable for wet chemical synthesis of this kind of ferrite. Simultaneously, hexagonal ferrite has a high optical absorption coefficient, but its charge carrier transfer and separation efficiency is low, which is not conducive to photocatalytic degradation of pollutants. Therefore, researchers are forced to use special preparation methods to improve the charge carrier transfer and separation efficiency of pure phase $MFe_{12}O_{19}$, and at the same time to enhance the charge carrier transfer and separation efficiency of $MFe_{12}O_{19}$ photocatalyst through ion doping and multi-component semiconductor coupling. The photocatalytic activity of

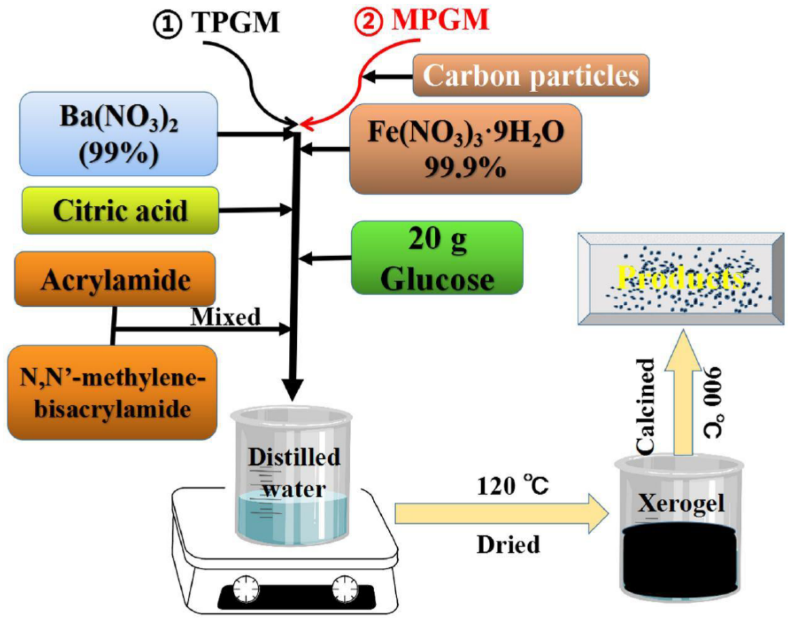

Figure 2: The synthetic path diagram of $BaFe_{12}O_{19}$ nanoparticles prepared by different polyacrylamide gel methods. Adapted from ref. [48]. Copyright © 2021 Trans Tech Publications Ltd.

$MFe_{12}O_{19}$ photocatalyst will be greatly affected by different preparation methods. It is worth noting that different ion doping and different semiconductor coupling of $MFe_{12}O_{19}$ photocatalyst will lead to different photocatalytic activity of $MFe_{12}O_{19}$ photocatalyst.

2.1. Synthesis of Single Phase $MFe_{12}O_{19}$ Photocatalysts

There are many methods to synthesize $MFe_{12}O_{19}$ photocatalyst, including solid phase reaction method, hydrothermal method, coprecipitation method, electrospinning method, sol-gel method and so on. Solid phase reaction method uses simple raw materials, not easy to introduce impurities, but its high synthesis temperature, the equipment requirements are relatively harsh, and the synthesized particle size is large, limiting the application of $MFe_{12}O_{19}$ in the field of photocatalysis. [43] High temperature reaction method can use oxides as raw materials, but it is exothermic reaction, the heat generated is easy to harm the equipment and human body, so this method limits its application in the preparation of $MFe_{12}O_{19}$. [44] Hydrothermal method has relatively low requirements on temperature and equipment, and only requires a reactor to generate pressure below 300 °C to generate the target product. However, the yield is very low and the synthesis time is long, which makes the preparation of $MFe_{12}O_{19}$ photocatalyst often need to spend a lot of time and raw materials. [45] Similar to hydrothermal method, coprecipitation method has low synthesis temperature but low yield, so its application in the synthesis of photocatalysts is limited. [46] It is easy to obtain nanowire or nanorods by electrospinning method, but the high pressure is dangerous and the improper operation can easily cause injury. [47] Sol-gel method is a kind of method which can adjust experimental parameters to obtain different morphology, phase purity and physical and chemical properties of $MFe_{12}O_{19}$ photocatalysts. It is the mainstream method for the synthesis of $MFe_{12}O_{19}$ photocatalysts. [19] Recently, the $MFe_{12}O_{19}$ nanoparticles have been synthesized by our group using both traditional polyacrylamide gel method (TPGM) and modified polyacrylamide gel method (MPGM), as shown in Figure **2**. By adjusting the sintering temperature, $MFe_{12}O_{19}$ with different morphologies can be obtained easily. [26, 48-50] The highly dispersed $MFe_{12}O_{19}$ particles were easily obtained by introducing glucose into the precursor solution.

2.2. Synthesis of Ion Doped $MFe_{12}O_{19}$ Photocatalysts

In the process of synthesizing ion-doped $MFe_{12}O_{19}$ photocatalyst, it is necessary to consider the content of doping ions, too much will form impurity oxides of doping ions, so that doping ions cannot occupy the position of $MFe_{12}O_{19}$ lattice. To obtain the best doping ratio, researchers are constantly improving synthesis methods to synthesize ion-doped $MFe_{12}O_{19}$ photocatalysts. The synthesis of ion-doped $MFe_{12}O_{19}$ photocatalyst is far more complex than that of single-

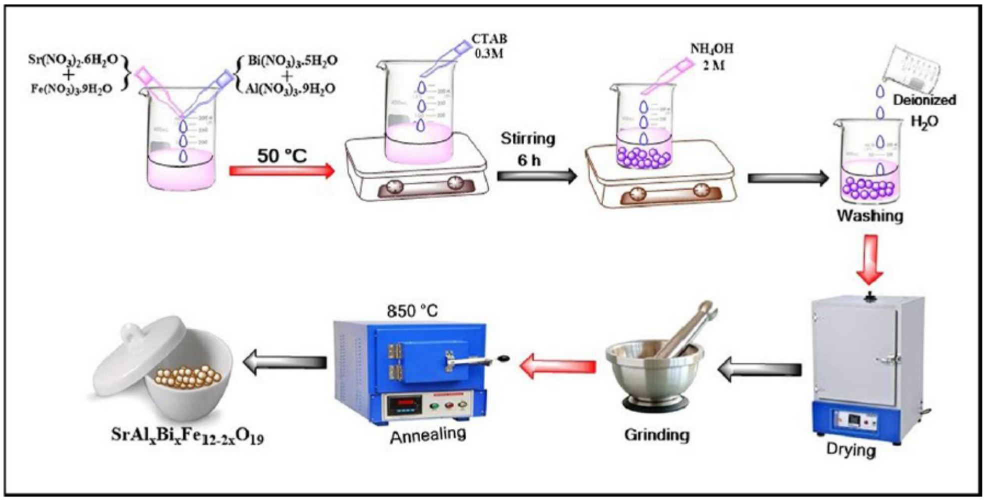

Figure 3: Preparation flow chart for the synthesis of $SrAl_xBi_xFe_{12-2x}O_{19}$ nanoparticles prepared via facile micro-emulsion method. Adapted from ref. [58]. Copyright © 2022 The Korean Society of Industrial and Engineering Chemistry. Published by Elsevier B.V.

phase $MFe_{12}O_{19}$ photocatalysts, and the conventional synthesis method is easy to introduce impurities, and it is difficult to obtain the desired target products, which will enable researchers to constantly develop new methods to synthesize ion-doped $MFe_{12}O_{19}$ photocatalysts. A simple microemulsion method was developed to synthesize a variety of ion-doped $MFe_{12}O_{19}$ photocatalysts, including $Ba_{1-x}Nd_xFe_{12-y}Cu_yO_{19}$, [51] $Ba_{1-x}Co_xFe_{12-y}Cr_yO_{19}$, [52] $BaNi_xFe_{12-x}O_{19}$, [53] $Ba_{1-x}Zn_xFe_{12-y}Cr_yO_{19}$, [54] $BaCr_xFe_{12-x}O_{19}$, [33] $Ba_{1-x}Zn_xFe_{12-y}Mn_yO_{19}$, [55] $Sr_{1-x}Zn_xFe_{1-y}Ni_yO_{19}$, [56] and $Ba_{1-x}Mg_xFe_{12-y}Mn_yO_{19}$ [57]. Raza *et al*. [58] reported the $SrAl_xBi_xFe_{12-2x}O_{19}$ nanoparticles prepared via facile micro-emulsion method exhibits high photocatalytic activity and antibacterial properties. The preparation flow chart for the synthesis of $SrAl_xBi_xFe_{12-2x}O_{19}$ nanoparticles as shown in Figure **3**. First, the corresponding metal salts are dissolved in deionized water in molar ratio. Subsequently, cetyltrimethylammonium bromide was added to reduce superfacial tension and reduce rapid agglomeration between particles. After all reagents are completely dissolved, the pH value is adjusted with ammonia water, and the final product is obtained after several times of cleaning, drying, ball milling and sintering. Ashraf *et al*. [59] also synthesized $Ba_{0.4}Sr_{0.6}Al_{0.4-x}Sm_xFe_{11.60}O_{19}$ photocatalysts by the sol-gel method, which showed high photocatalytic activity in the degradation of methylene blue.

2.3. Synthesis of $MFe_{12}O_{19}$ Based Composite Photocatalysts

For the $MFe_{12}O_{19}$-based multi-element composite photocatalysts, in addition to obtaining single-phase matrix material, it is necessary to construct multi-element composite photocatalysts. There are three common methods. First, each single-phase catalyst is synthesized in a different way, and then a variety of single-phase materials are coupled together by a special synthesis method. [27, 28, 60, 61] Zhang *et al*. [36] synthesized $BaFe_{12}O_{19}/Bi_{3.64}Mo_{0.36}O_{6.55}$ composite photocatalysts by the low temperature sintering technology combined with hydrothermal method, the photocatalyst shows a high photocatalytic activity for the degradation of pollutants. Figure **4** shows the synthetic process of $BaFe_{12}O_{19}/Bi_{3.64}Mo_{0.36}O_{6.55}$ composite photocatalysts. By this method, the fine particles of $Bi_{3.64}Mo_{0.36}O_{6.55}$ were successfully interacted on the lamellar $BaFe_{12}O_{19}$ photocatalysts. Such binding mode promotes the transfer and separation of charge carriers at the interface of $BaFe_{12}O_{19}$ and $Bi_{3.64}Mo_{0.36}O_{6.55}$, thus enhancing the photocatalytic activity of the system. The second is to synthesize a single phase material and then coupled another single phase material together in the same way. [34, 62, 63] This method is simpler and more efficient than the previous method and reduces the influence of the intermediate process on the properties of the final product. The third method is one-step synthesis method. [64-66] This method is to add different metal salts to the precursor solution at one time according to the molar ratio, and obtain the final product through gel, drying and sintering. Although the one-step synthesis method is very simple compared with the previous two methods, the composition is difficult to control, so there are not many researchers who use this method to synthesize $MFe_{12}O_{19}$-based composite photocatalysts.

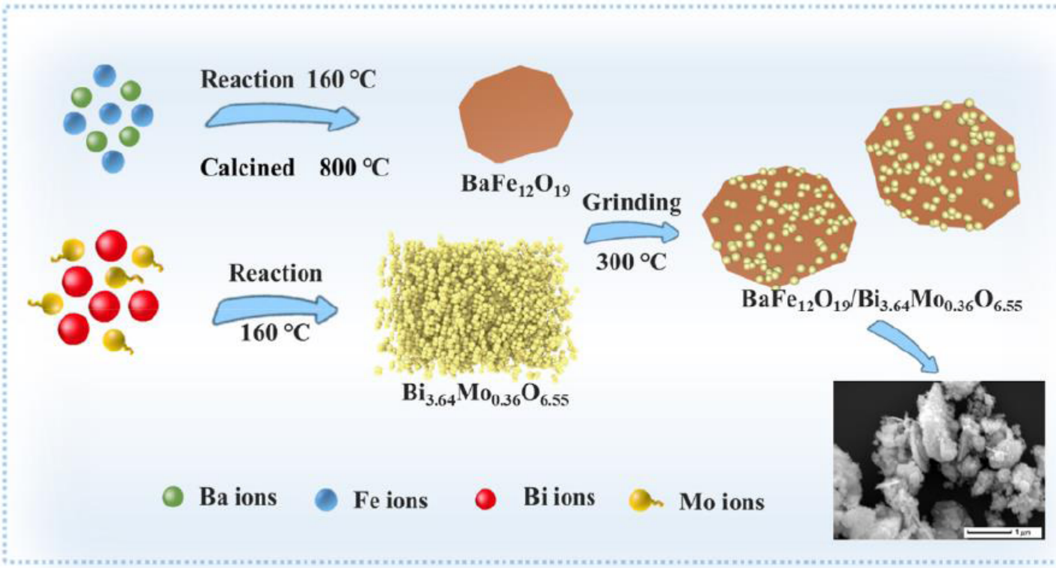

Figure 4: The synthetic process of $BaFe_{12}O_{19}/Bi_{3.64}Mo_{0.36}O_{6.55}$ composite photocatalysts. Adapted from ref. [36]. Copyright © 2022 Elsevier Ltd.

3. PHOTOCATALYTIC APPLICATIONS

With high optical absorption coefficient and magnetic properties, $MFe_{12}O_{19}$ has important applications in the field of magnetic separation recyclable photocatalysis. However, as a photocatalyst, $MFe_{12}O_{19}$ is not the most excellent photocatalytic semiconductor materials due to its high charge carrier recombination rate. In terms of magnetic separation and recovery, $MFe_{12}O_{19}$'s high magnetic properties make it better than other semiconductor magnetic materials in this field. Due to the application of $MFe_{12}O_{19}$ photocatalyst in magnetic separation and recovery, many types of photocatalysts have been gradually developed, including ion-doped $MFe_{12}O_{19}$ photocatalysts, multi-heterojunction $MFe_{12}O_{19}$-based composite photocatalysts, etc. These new magnetic separation photocatalysts have been widely used in the degradation of dyes, drugs and POPs.

3.1. Applications in the Degradation of Dyes

Most of the $MFe_{12}O_{19}$-based photocatalysts for the degradation of pollutants are mainly concentrated in the degradation of dye, especially the color dye to the river pollution is shocking. Table **2** shows the photocatalytic activity of $MFe_{12}O_{19}$-based composite photocatalysts toward the photodegradation of dyes. Single-phase $MFe_{12}O_{19}$ photocatalyst can degrade dyes, but the degradation effect is not as good as that of ion-doped $MFe_{12}O_{19}$ photocatalysts and multiplex $MFe_{12}O_{19}$ composite photocatalysts. Compared with the $MFe_{12}O_{19}$ photocatalyst, the optical band gap value of the ion-doped $MFe_{12}O_{19}$ photocatalyst is significantly reduced, which also makes the ion-doped $MFe_{12}O_{19}$ show more excellent photocatalytic activity. However, due to the presence of Fe ions, the photocatalytic mechanism of $MFe_{12}O_{19}$ based photocatalyst is unclear. After years of unremitting research, the photocatalytic mechanism of $MFe_{12}O_{19}$ based photocatalyst was finally revealed. Simultaneously, the photocatalytic activity of $MFe_{12}O_{19}$-based photocatalysts is affected by the type of dye, light time, dye concentration, catalyst content, light source and other factors, so that they show different photocatalytic activity. [67-104] The photocatalytic activity of ion doped $MFe_{12}O_{19}$ photocatalysts is affected by doping ions, which contribute a lot to photocatalysis, which makes the analysis of its photocatalysis mechanism also greatly affected. In the construction of multi-heterojunction $MFe_{12}O_{19}$ composite photocatalysts, its photocatalytic activity is affected by other semiconductor materials, so the selection of semiconductor materials is very careful. Researchers have combined oxides, sulfides, polymers, metal-organic framework materials, carbon nanotubes, noble metal particles with $MFe_{12}O_{19}$ to construct $MFe_{12}O_{19}$-based composite photocatalysts, which have been widely used in the degradation of organic dye wastewater. [40, 46, 67, 73, 74] To make $MFe_{12}O_{19}$-based photocatalyst practical, researchers have been trying to combine $MFe_{12}O_{19}$ with other substances to obtain $MFe_{12}O_{19}$-based composite photocatalysts with excellent photocatalytic activity.

Table 2: The photocatalytic activity of $MFe_{12}O_{19}$-based composite photocatalysts toward the photodegradation of dyes. MB -Methylene Blue, ABU Acid blue, ABA-Acid black, AV-Acid violet, ABR-Acid brown, ES -Eosin, CR-Congo red, CV-Sulphur blue, AR -Acid red, MG -Malachite green, MO -Methyl orange, MR-Methyl red, MW-Methylene white, TB-Toluidine blue, MX-5B - Procion red, BR46-Basic Red 46, RhB - Rhodamine B

Samples	Dye	Lamp	$C_{Catalyst}$ ($g \cdot L^{-1}$)	C_{Drug} (mmol L^{-1})	t (h)	D (%)	SA (mmol/g/h)	Reference
$Ba_{1-x}Sm_xFe_{12-x}CoxO_{19}$	MB	Visible light	2.00	0.031	1	87.12%	0.0135	[63]
$BaFe_{12}O_{19}$	MB	Visible light	0.75	0.031	6	70.8%	0.0048	[32]
$Ba_{0.4}Sr_{0.6}Al_{0.4-x}Sm_xFe_{11.60}O_{19}$	MB	UV light	0.25	0.031	2.34	99%	0.0525	[59]
$BaFe_{12}O_{19}/Sm_2Ti_2O_7$/Ag	MB	Osram lamp	/	0.031	2	99.03%	/	[67]
$BaFe_{12}O_{19}$	MB	Xenon lamp	2.00	0.031	3	78%	0.0041	[68]
$BaFe_{12}O_{19}$	MB	Sun light	0.80	0.125	3	73%	0.038	[69]
$CuFe_{12}O_{19}$-CNT	MB	UV light	0.02	0.063	0.83	54.1%	2.0531	[40]
$SrFe_{12}O_{19}$	MB	Xenon lamp	1.00	0.031	4.5	95%	0.0065	[70]
$ZnFe_2O_4/SrFe_{12}O_{19}$	MB	Xenon lamp	2.00	0.031	2	96.6%	0.0075	[64]
$SrFe_{12}O_{19}/MoS_2$	MB	Visible light	0.40	0.063	1	86%	0.1354	[46]
$SrFe_{12}O_{19}$	MB	Visible light	4.00	0.016	3	84%	0.0011	[71]
$SrFe_{12}O_{19}/ZnFe_2O_4$	MB	Visible light	1.00	0.016	4	90%	0.0036	[65]
$SrFe_{12}O_{19}$	MB	UV light	/	0.156	2	46%	/	[72]
MIL-88A (Fe)/BiOBr/$SrFe_{12}O_{19}$	MB	Xenon lamp	1.00	0.031	1.5	90.1%	0.0186	[73]
$Sr(CeNd)_xFe_{12-2x}O_{19}$/polythiophene	MB	Mercury lamp	2.00	0.031	0.5	98%	0.0304	[74]
$La_{0.2}Sr_{0.7}Fe_{12}O_{19}$	MB	Xenon lamp	1.00	0.031	6	88%	0.0045	[75]
$SrFe_{12}O_{19}/SiO_2$ $/TiO_2$	MB	UV light	/	0.156	3	83%	/	[76]
$SrFe_{12}O_{19}/SiO_2/TiO_2$	MB	UV light	/	0.156	3	80%	/	[77]
15%$SrFe_{12}O_{19}/BiVO_4$	MB	Xenon lamp	2.00	0.016	5	93%	0.0015	[78]
$ZnFe_2O_4$-$SrFe_{12}O_{19}$	MB	Halogen lamp	2.00	0.031	5	100%	0.0031	[66]
TiO_2-coated $SrFe_{12}O_{19}$	MB	UV light	0.18	0.078	7	98.19%	0.0625	[79]
25%$SrFe_{12}O_{19}/SrTiO_3$	MB	Xenon lamp	0.67	0.013	2	98.6%	0.0096	[80]
$Bi_2O_3/SrFe_{12}O_{19}$	MB	Halogen lamp	2.00	0.013	4/6	97.7%	0.0016	[41]
BiOCl-$SrFe_{12}O_{19}$	MB	UV light	2.00	0.013	0.83	99%	0.0077	[81]
$TiO_2/SrFe_{12}O_{19}$	MB	UV light	2.00	0.013	5	94.7%	0.0012	[82]
$BaFe_{12}O_{19}$–TiO_2	AB	UV light	10.00	0.021	1	/	/	[83]
$PbFe_{12}O_{19}$-TiO_2	ABU	UV light	20.00	0.021	1	75%	0.0009	[24]
$PbFe_{12}O_{19}$-PbS	ABU	UV light	10.00	0.042	1	97%	0.0041	[25]
$SrFe_{12}O_{19}$@Ag	ABU	Tungsten lamp	1.00	0.011	2	58.1%	0.0032	[84]
$BaFe_{12}O_{19}$–ZnO	ABA	UV light	10.00	0.016	1	81%	0.0013	[85]
$SrFe_{12}O_{19}$–$SrTiO_3$	ABA	UV light	10.00	/	0.5	95%	/	[86]
$CoFe_2O_4/BaFe_{12}O_{19}$	CR	Xenon lamp	5.00	/	0.83	84.5%	/	[38]
$SrFe_{12}O_{19}$	CR	Visible light	0.50	0.028	3	90%	0.0168	[87]
$Ba_{1-x}Co_xFe_{12-y}Cr_yO_{19}$	CV	Sun light	0.10	0.024	1	64.23%	0.1541	[52]
$BaNi_xFe_{12-x}O_{19}$	CV	Xenon lamp	0.07	0.024	1.7	97%	0.2044	[53]
$BaCr_xFe_{12-x}O_{19}$	CV	Argon lamp	0.10	0.024	1.5	91%	0.1456	[33]

$SrBi_xAl_xFe_{12-2x}O_{19}$	CV	Sun light	1.00	0.024	2	83%	0.0099	[58]
$SrMn_xFe_{12-x}O_{19}$	CV	Sun light	0.10	0.024	1.67	96%	0.1497	[88]
$SrNi_xFe_{12-x}O_{19}$	CV	Visible light	0.02	0.024	1.5	91%	0.728	[89]
$CuFe_{12}O_{19}$ /CNT	AR	UV light	0.02	0.023	0.83	21.6%	0.2953	[29]
$Ba_{1-x}Nd_xFe_{12-y}Cu_yO_{19}$	MG	Sun light	0.05	0.011	1	92.6%	0.2	[51]
$BaFe_{12}O_{19}/Bi_{3.64}Mo_{0.36}O_{6.55}$	MO	Visible light	0.20	0.062	1	84.5%	0.2619	[36]
$BaFe_{12}O_{19}$	MO	Visible light	0.50	0.031	0.67	97%	0.0898	[90]
$BaFe_{12}O_{19}$	MO	Hg lamp	2.00	/	3.3	95%	/	[91]
$PbFe_{12}O_{19}$	MO	UV light	/	/	1.17	29.41%	/	[22]
$SrFe_{12}O_{19}/MoS_2$	MO	Visible light	0.40	0.062	1	61%	0.0946	[92]
$SrFe_{12}O_{19}$	MO	Hg lamp	2.00		3.67	95%		[93]
$SrFe_{12}O_{19}$	TB	Tungsten lamp	5.00	0.100	20h	100%	0.001	[94]
$TiO_2/BaFe_{12}O_{19}$	MX-5B	UV light	0.01	/	5	96%	/	[95]
$SrFe_{12}O_{19}/ZnO$	BR46	Visible light	0.75	0.025	1.5	99%	0.022	[96]
16.8%of$BaFe_{12}O_{19}/g\text{-}C_3N_4$	RhB	Visible light	1.00	0.021	1.7	95.8%	0.0118	[61]
10% $BaFe_{12}O_{19}/AgBr$	RhB	Xenon lamp	0.50	0.042	0.5	98.2%	0.1649	[62]
$Ba_{1-x}Zn_xFe_{12}\text{-}yCr_yO_{19}$	RhB	Sun light	/	/	1.5	81.8%	/	[54]
$BaFe_{12}O_{19}$	RhB	Xenon lamp	20.00	0.021	3	100%	0.0004	[97]
$Ba_{1-x}Mg_xFe_{12-y}Mn_yO_{19}$	RhB	Sun light	0.10	0.021	0.83	85%	0.2151	[57]
$BiOC_l/SrFe_{12-x}Co_xO_{19}/rGO$	RhB	Sun light	1.00	0.021	1.33	94%	0.0148	[98]
$Bi_3O_4Cl/SrFe_{12}O_{19}$	RhB	Sun light	1.00	0.021	1.33	99.7%	0.0157	[40]
$Bi_4O_5Br_2/SrFe_{12}O_{19}$	RhB	Xenon lamp	1.00	0.021	1	99.3%	0.0209	[99]
$ZnO/SrFe_{12}O_{19}$	RhB	Xenon lamp	1.00	0.021	1.17	99.5%	0.0178	[100]
$\beta\text{-}Bi_2O_3/SrFe_{12}O_{19}$	RhB	Xenon lamp	2.00	0.021	2.5	92.97%	0.0039	[41]
$ZnO/Bi_{24}O_{31}Br_{10}@SrFe_{12}O_{19}$	RhB	Xenon lamp	0.50	0.042	0.5	96.8%	0.1626	[101]
$Sr_{1-x}Co_xFe_{12-y}Cr_yO_{19}$	RhB	Sun light	0.10	0.021	0.75	87.6%	0.2453	[102]
$BiOBr/SrFe_{12}O_{19}$	RhB	Visible light	0.50	0.021	0.5	97%	0.0814	[103]
$BiOCl/SrFe_{12-x}CoxO_{19}$	RhB	Xenon lamp	1.00	0.021	1.67	98%	0.0123	[104]

3.2. Applications in the Degradation of Drugs

Recently, the research of $MFe_{12}O_{19}$-based photocatalysts in the degradation of dyes is becoming more and more mature. No new breakthrough can be made in the degradation process, the influence of process parameters or the study of photocatalytic mechanism, which makes researchers have to open up new ways to study the photocatalytic activity of $MFe_{12}O_{19}$-based photocatalysts. Drugs contain a large number of antibiotics, and only a small part of them are absorbed by human body, animal and aquatic products. Most of them will be discharged through feces and other excretions, thus polluting the environment. Using this as a breakthrough, researchers have made a certain breakthrough in drug degradation of $MFe_{12}O_{19}$-based photocatalysts. Table **3** shows the photocatalytic activity of $MFe_{12}O_{19}$-based composite photocatalysts toward the photodegradation of drugs. Kaur *et al*. [105] decorated different metal ions such as Cr, Mn, Fe, Co. Ni. Cu, Zn on the surface of $SrFe_{12}O_{19}$ and studied the effect of these ions on the degradation of levofloxacin (LVX) and sulfamethoxazole (SFX). The results showed that the $SrFe_{12}O_{19}$-based photocatalyst was selective to drug degradation, and its photocatalytic activity was affected by metal ions. Other novel $MFe_{12}O_{19}$-based photocatalysts have also been used to degrade drugs. [20, 34, 36, 37, 106-109] The research on the degradation of drugs is still in the stage of vigorous development. Many photocatalytic mechanisms are unknown, and advanced technologies are needed to

Table 3: The photocatalytic activity of $MFe_{12}O_{19}$-based composite photocatalysts toward the photodegradation of drugs. LVX - Levofloxacin, SFX - Sulfamethoxazole, RDX - hexahydro-1,3,5- trinitro-1,3,5 triazine, OC - Oxytetracy cline, CC - Chlortetracycline, TCH - Tetracycline Hydrochloride, TC - Tetracycline, CFX - Ceftriaxone sodium, BPA - bisphenol A, ATZ- Atrazine, 2.4-DCP - 2,4-Dichlorophenol

Samples	Drug	Lamp	$C_{Catalyst}$ ($g \cdot L^{-1}$)	C_{Drug} (mmol L^{-1})	t (h)	D (%)	SA (mmol/g/h)	Reference
$SrFe_{12}O_{19}$	LVX	Visible light	0.5	0.05	2	64.5%	0.03225	[105]
$SrFe_{12}O_{19}$@Dop	LVX	Visible light	0.5	0.05	2	71.5%	0.03575	
$SrFe_{12}O_{19}$@Dop@Cr	LVX	Visible light	0.5	0.05	2	68.5%	0.03425	
$SrFe_{12}O_{19}$@Dop@Mn	LVX	Visible light	0.5	0.05	2	98.1%	0.04905	
$SrFe_{12}O_{19}$@Dop@Fe	LVX	Visible light	0.5	0.05	2	92%	0.046	
$SrFe_{12}O_{19}$@Dop@Co	LVX	Visible light	0.5	0.05	2	95.2%	0.0476	
$SrFe_{12}O_{19}$@Dop@Ni	LVX	Visible light	0.5	0.05	2	95.3%	0.04765	
$SrFe_{12}O_{19}$@Dop@Cu	LVX	Visible light	0.5	0.05	2	94.5%	0.04725	
$SrFe_{12}O_{19}$@Dop@Zn	LVX	Visible light	0.5	0.05	2	93.1%	0.04655	
$SrFe_{12}O_{19}$	SFX	Visible light	0.5	0.05	2	66%	0.033	
$SrFe_{12}O_{19}$@Dop	SFX	Visible light	0.5	0.05	2	72.1%	0.0361	
$SrFe_{12}O_{19}$@Dop@Cr	SFX	Visible light	0.5	0.05	2	70.7%	0.0353	
$SrFe_{12}O_{19}$@Dop@Mn	SFX	Visible light	0.5	0.05	2	97.2%	0.0486	
$SrFe_{12}O_{19}$@Dop@Fe	SFX	Visible light	0.5	0.05	2	84.1%	0.0421	
$SrFe_{12}O_{19}$@Dop@Co	SFX	Visible light	0.5	0.05	2	95.6%	0.0478	
$SrFe_{12}O_{19}$@Dop@Ni	SFX	Visible light	0.5	0.05	2	89.2%	0.0446	
$SrFe_{12}O_{19}$@Dop@Cu	SFX	Visible light	0.5	0.05	2	92.9%	0.0465	
$SrFe_{12}O_{19}$@Dop@Zn	SFX	Visible light	0.5	0.05	2	75.2%	0.0376	
$BaFe_{12}O_{19}$-(800℃)	RDX	UV light	1	0.1801	4	98.1%	0.0441	[106]
$BaFe_{12}O_{19}/Bi_{3.64}Mo_{0.36}O_{6.55}$	OC	Visible light	0.2	0.043	1	86%	0.1849	[36]
$BaFe_{12}O_{19}/Bi_{3.64}Mo_{0.36}O_{6.55}$	CC	Visible light	0.2	0.0417	1	81%	0.1688	
$BaFe_{12}O_{19}/Bi_{3.64}Mo_{0.36}O_{6.55}$	TCH	Visible light	0.2	0.042	1	84.5%	0.1775	
$Bi_2O_3/Bi_2S_3/BaFe_{12}O_{19}$	TC	Visible light	3	0.022	1	83%	0.0061	[107]
$NiFe_{12}O_{19}$-ZnO	CFX	UV light	0.4	0.0523	2	98.5%	0.0644	[20]
$NiFe_{12}O_{19}-TiO_2$	CFX	UV light	0.2	0.0523	2	95.5%	0.1248	
$NiFe_{12}O_{19}$	CFX	UV light	/	/	2	74.7%	/	
1%$BaFe_{12}O_{19}/Ag_3PO_4$	BPA	Xenon lamp	1	0.0876	0.5	53.3%	0.0933	[37]
5%$BaFe_{12}O_{19}/Ag_3PO_4$	BPA	Xenon lamp	1	0.0876	0.5	65.3%	0.1144	
10%$BaFe_{12}O_{19}/Ag_3PO_4$	BPA	Xenon lamp	1	0.0876	0.5	79.9%	0.1399	
15%$BaFe_{12}O_{19}/Ag_3PO_4$	BPA	Xenon lamp	1	0.0876	0.5	79.8%	0.1398	
$Ag_2O/BaFe_{12}O_{19}$	ATZ	Xenon lamp	1	0.2318	1	74%	0.1715	[34]
0.4%$Ag_2O/BaFe_{12}O_{19}$	ATZ	Xenon lamp	1	0.2318	1	79%	0.1831	
0.8%$Ag_2O/BaFe_{12}O_{19}$	ATZ	Xenon lamp	1	0.2318	1	90%	0.2086	
1.2%$Ag_2O/BaFe_{12}O_{19}$	ATZ	Xenon lamp	1	0.2318	1	100%	0.2318	
$TiO_2-SiO_2-BaFe_{12}O_{19}$	2.4-DCP	Sun light	/	/	2.5	100%	/	[108]
$TiO_2/GO/SrFe_{12}O_{19}$	2.4-DCP	Sun light	4	0.3067	3	100%	0.0256	[109]

characterize the degradation processes to gain an in-depth insight into their photocatalytic mechanisms.

3.3 Applications in the Degradation of POPs

There are few studies on the degradation of POPs

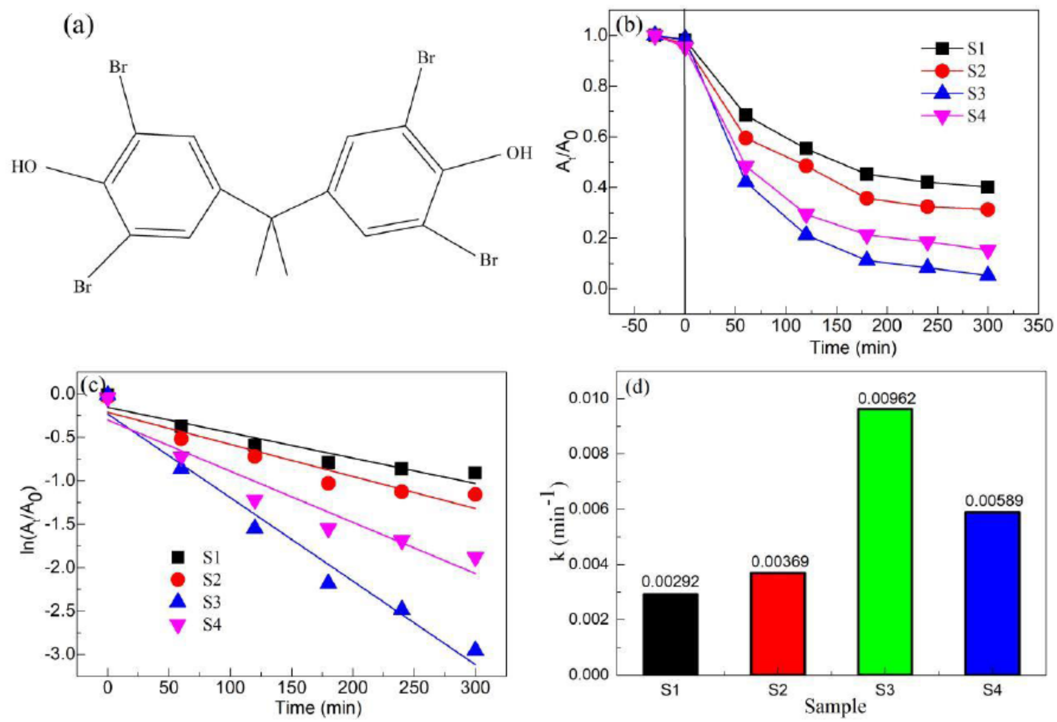

Figure 5: (**a**) Molecular structure of tetrabromobisphenol A. (**b**) Photocatalytic degradation curve, (**c**) Plots of $\ln(A_t/A_0)$ vs. irradiation time and (**d**) First order kinetic constant (**k**) of tetrabromobisphenol A in the presence of of carbon quantum dots (CQDs)/CeO_2/$BaFe_{12}O_{19}$ magnetic separation photocatalysts under simulated sunlight radiation. S1-CeO_2, S2-(15 wt%) CQDs / (5 wt% $BaFe_{12}O_{19}$/CeO_2), S3-(15 wt%) CQDs / (10 wt% $BaFe_{12}O_{19}$/CeO_2) and S4-(15 wt%) CQDs / (15 wt% $BaFe_{12}O_{19}$/CeO_2). Adapted from ref. [28]. Copyright © 2022 The Authors. Publishing services by Elsevier B.V. on behalf of KeAi Communications Co. Ltd.

by $MFe_{12}O_{19}$. Tetrabromobisphenol is a type of POPs, which is very harmful to the environment. In our early study, the CQDs/CeO_2/$BaFe_{12}O_{19}$ magnetic separation photocatalysts was synthesized by the hydrothermal method combined with the polyacrylamide gel method, and the photocatalytic activity of the magnetic separation photocatalysts for the degradation of tetrabromobisphenol under visible light irradiation was studied. CeO_2 is easily synthesized by wet chemistry and its particle size can be easily controlled. [110] Due to its internal oxygen vacancy, CeO_2 is very popular for photocatalytic degradation of pollutants.The effects of different contents of CQDs and $BaFe_{12}O_{19}$ on the photocatalytic activity of CQDs/CeO_2/$BaFe_{12}O_{19}$ magnetic separation photocatalyst were studied. The photocatalytic activity of CQDs/CeO_2/$BaFe_{12}O_{19}$ magnetic separation photocatalyst can be effectively regulated by magnetic field. Figure **5** shows the molecular structure of tetrabromobisphenol A and the photocatalytic activity of CQDs/CeO_2/$BaFe_{12}O_{19}$ magnetic separation photocatalysts. It can be seen from Figure **5** that the CQDs/CeO_2/$BaFe_{12}O_{19}$ magnetic separation photocatalysts has the best photocatalytic activity to degrade tetrabromobisphenol A when the mass percentage of $BAFe_{12}O_{19}$ is 10 wt%. Due to the small content of carbon quantum dots and $BaFe_{12}O_{19}$ in CQDs/CeO_2/$BaFe_{12}O_{19}$ magnetic separation photocatalysts, it is very difficult to detect them by conventional XRD. Therefore, neutron powder diffraction is used to study their composition, phase structure and magnetic structure. The FENGHUANG diffractometer is very suitable for measuring the neutron powder diffraction spectra of magnetic samples at different temperatures. [111] In the study of other low content $MFe_{12}O_{19}$ composite photocatalysts, it is important to use neutron powder diffraction to understand its phase composition, structure and magnetic structure.

4. PHOTOCATALYTIC MECHANISM

Since $MFe_{12}O_{19}$ was used as a photocatalyst, the research on it has been non-stop. Due to the high magnetic properties of $MFe_{12}O_{19}$, it can be separated from water by magnetic field when it is used as a photocatalyst, without causing secondary pollution to water. However, the charge transfer and separation efficiency of single-phase $MFe_{12}O_{19}$ is low, which makes its application as a photocatalyst very limited. Therefore, researchers have adopted various methods to improve the photocatalytic activity of $MFe_{12}O_{19}$. After

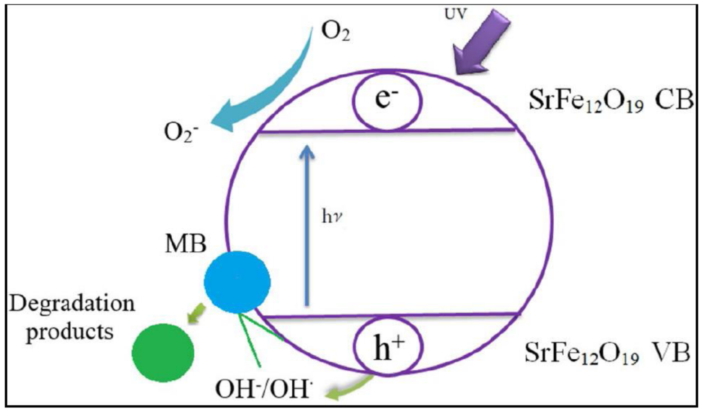

Figure 6: Photocatalysis mechanism of $SrFe_{12}O_{19}$ particles. Adapted from ref. [72]. Copyright © Springer Science+Business Media, LLC, part of Springer Nature 2020.

years of research, a unified theory of photocatalysis mechanism has been preliminarily formed.

4.1. Photocatalytic Mechanism of Single Phase $MFe_{12}O_{19}$ Photocatalysts

The optical bandgap value of $MFe_{12}O_{19}$ is affected by M ions, but they have high optical absorption coefficients in both ultraviolet and visible ranges. The high optical absorption coefficient of visible light makes it possible for $MFe_{12}O_{19}$ to respond to visible light during photocatalytic degradation of pollutants. Figure **6** shows the photocatalysis mechanism of $SrFe_{12}O_{19}$ particles. [72] When a beam of light with an energy greater than the optical bandgap value of $MFe_{12}O_{19}$ shines on its surface, electrons in the valence band (VB) of $MFe_{12}O_{19}$ will transition to its conduction band (CB), leaving holes in the valence band. The holes in the valence band will react with water in the reaction solution to form hydroxyl radicals. The conduction electrons will react with the oxygen in the reaction solution to form a superoxide radical. Hydroxyl radicals and superoxide radicals react with pollutants to produce non-toxic and harmless products. [93] However, when the optical bandgap value of $MFe_{12}O_{19}$ is large, it is difficult for $MFe_{12}O_{19}$ to respond to visible light, which will result in low photocatalytic activity of $MFe_{12}O_{19}$ in visible light.

4.2. Photocatalytic Mechanism of Ion Doped $MFe_{12}O_{19}$ Photocatalysts

Ion doping $MFe_{12}O_{19}$ can effectively reduce its optical band gap value and improve its photocatalytic activity. For the photocatalyst with relatively large optical band gap in $MFe_{12}O_{19}$, this is undoubtedly good news in terms of enhancing its photocatalytic activity of visible light. Rasheed *et al*. [88] reported the Mn doped $SrFe_{12}O_{19}$ synthesized by a facile microemulsion route exhibits high solar-light-driven photocatalytic activity for the degradation of crystal violet dye. Figure **7** shows the photocatalysis mechanism of $SrMn_xFe_{12-x}O_{19}$

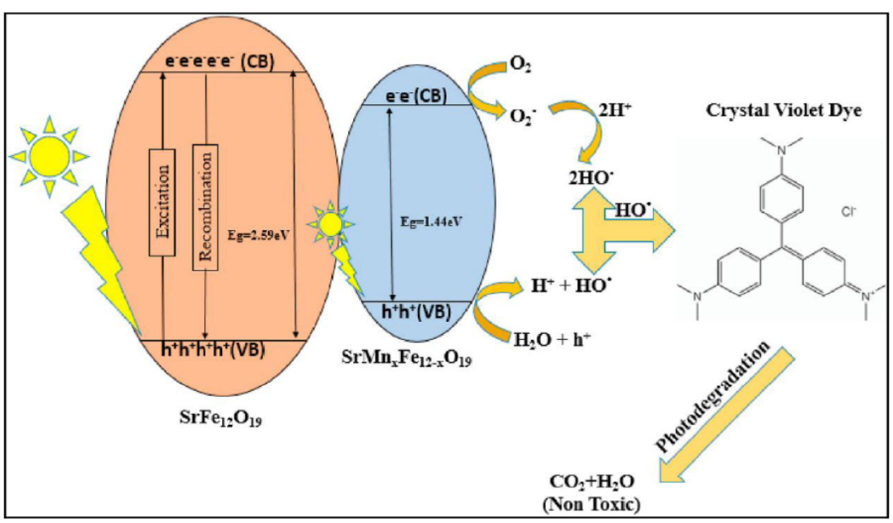

Figure 7: Photocatalysis mechanism of $SrMn_xFe_{12-x}O_{19}$ photocatalysts. Adapted from ref. [88]. Copyright © 2022 Elsevier B.V.

photocatalysts. When Mn ion is not incorporated, $SrFe_{12}O_{19}$ exhibits high charge carrier recombination rate, which makes its photocatalytic activity very poor. When Mn ions were introduced into $SrrFe_{12}O_{19}$, Mn ions occupied part of the position of Fe ions, so that the photocatalyst $SrMn_xFe_{12-x}O_{19}$ showed a lower optical band gap value than $SrFe_{12}O_{19}$, which enhanced the transmission ability between charge carriers. The photocatalytic activity of $SrMn_xFe_{12-x}O_{19}$ photocatalyst was significantly higher than that of $SrFe_{12}O_{19}$. The photocatalytic mechanism of $MFe_{12}O_{19}$ photocatalyst doped with metal ions is similar to that of single-phase $MFe_{12}O_{19}$ photocatalyst except that the optical band gap value is reduced [89, 112, 113].

4.3. Photocatalytic Mechanism of $MFe_{12}O_{19}$ Based Composite Photocatalysts

For the $MFe_{12}O_{19}$-based composite semiconductor photocatalysts, there are mainly three ways: One is the precious metal particles dotted on $MFe_{12}O_{19}$ photocatalysts; The other is the combination of other semiconductor materials and $MFe_{12}O_{19}$ photocatalysts; The other is the construction of multi-heterojunction $MFe_{12}O_{19}$ composite photocatalysts, which can effectively improve the transfer and separation of charge carriers between semiconductor interfaces. [64, 84, 98] In fact, these construction strategies are designed based on the theory of band arrangement. The type I band arrangement is conducive to the recombination of charge carriers, the type II band arrangement is conducive to the transfer and separation of charge carriers, and the ultrafine particles such as precious metal ions and carbon quantum dots act as the carriers of charge carrier transport in the process of photocatalyst degradation of pollutants. Figure **8** shows the photocatalysis mechanism of $MoS_2/SrFe_{12}O_{19}$ heterojunction photocatalysts. [64] A type II band arrangement is formed between MoS_2 and $SrFe_{12}O_{19}$, which effectively promotes the transfer and migration of electrons and holes at the interface between MOS_2 and $SrFe_{12}O_{19}$, thus improving the photocatalytic activity of $SrFe_{12}O_{19}$. Meanwhile, the conversion between Fe^{2+} and Fe^{3+} also greatly improves the transfer and separation of charge carriers, promotes the formation of superoxide free radicals, and thus accelerates the degradation of pollutants. [64, 92] In particular, the formation of p-n junction between $MFe_{12}O_{19}$ and another semiconductor helps to promote the photocatalytic activity of $MFe_{12}O_{19}$ semiconductor photocatalysts. [81] At the same time,

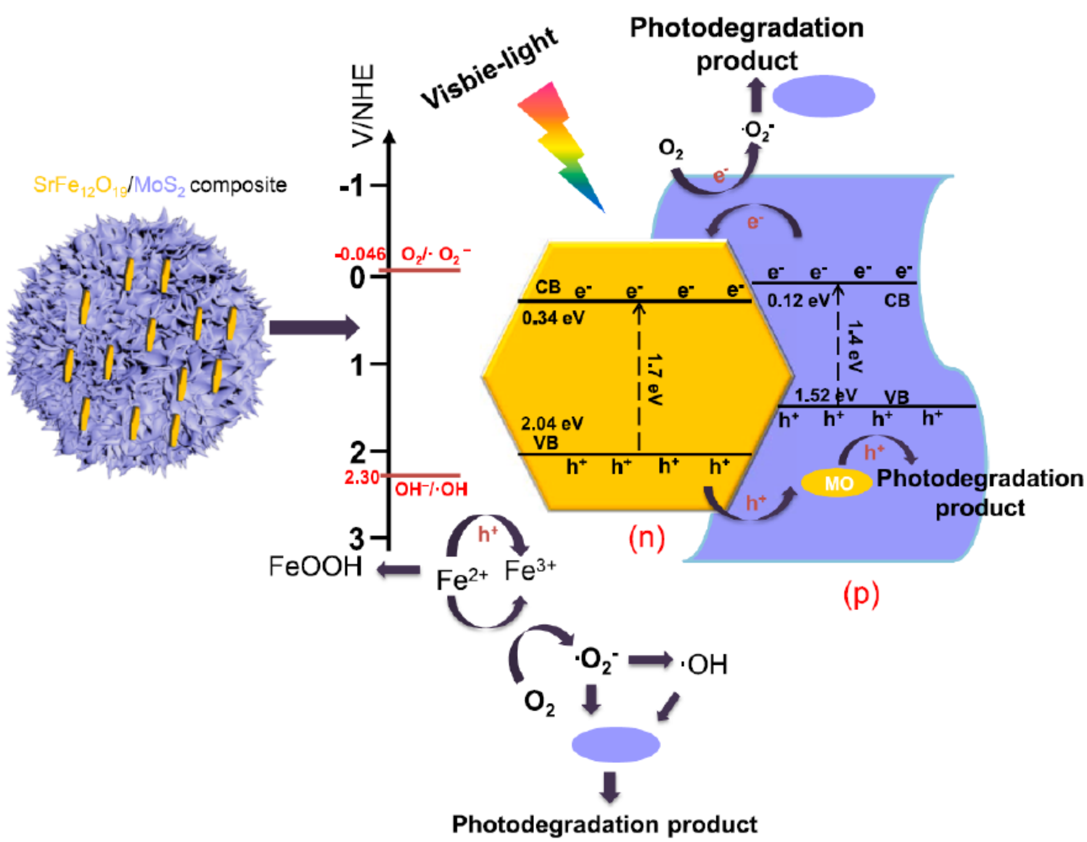

Figure 8: Photocatalysis mechanism of $MoS_2/SrFe_{12}O_{19}$ heterojunction photocatalysts. Adapted from ref. [64]. Copyright © 2021 Elsevier B.V.

the photocatalytic activity of $MFe_{12}O_{19}$ photocatalysts can also be enhanced by placing $MFe_{12}O_{19}$ photocatalysts into a metal-organic framework to form double Z-scheme heterojunction materials [73]. In addition to ion doping of $MFe_{12}O_{19}$, the researchers introduced a second phase of the semiconductor material for coupling, and also obtained a composite photocatalyst with high photocatalytic activity [74].

5. THE MECHANISM OF INTRINSIC CORRELATION BETWEEN PHOTOLUMINESCENCE AND PHOTOCATALYSIS

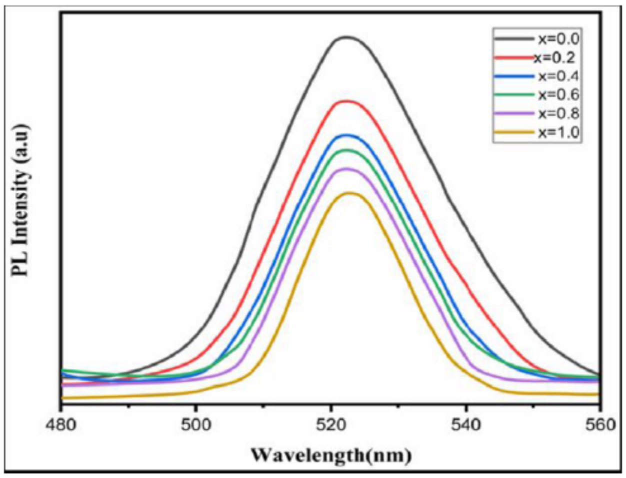

Figure 9: Emission spectra of $BaCr_xFe_{12-x}O_{19}$ nanoparticles. Adapted from ref. [33]. Copyright © 2022 The Author(s). Published by Elsevier B.V. on behalf of King Saud University.

Generally, the high photocatalytic activity of semiconductor materials is due to the transfer and separation of charge carriers resulting in the formation of a large number of free radicals in the reaction solution. These free radicals interact with pollutants to degrade the pollutants. The high photoluminescence properties of semiconductor materials are mainly due to the recombination of charge carriers, which causes the excess energy in the recombination process to be emitted in the form of photons, thus showing the photoluminescence properties. The photoluminescent properties of $MFe_{12}O_{19}$ are strongly dependent on the preparation method. A sol-gel autocombustion method has been used to synthesize $SrFe_{12}O_{19}$ nanomaterials, which exhibit a distinct emission peak at 350 nm under excitation wavelength at 270 nm. [114] $BaFe_{12}O_{19}$ synthesized by the same method showed a distinct emission peak at 605 nm. [115, 116] It can be seen that the photoluminescence properties of $MFe_{12}O_{19}$ are obviously different with the same preparation method but different M ions. To gain an insight into the internal correlation between photoluminescence and photocatalysis, Bibi *et al*. [33] synthesized a Cr-doped $BaFe_{12}O_{19}$ by a facile micro-emulsion route. Figure **9** shows the emission spectra of $BaCr_xFe_{12-x}O_{19}$ nanoparticles. With the increase of x content, the intensity of emission peak of $BaCr_xFe_{12-x}O_{19}$ nanoparticles decreased. The photocatalytic activity of $BaCr_xFe_{12-x}O_{19}$ nanoparticles increased with the increase of x value. It can be seen that the photocatalytic activity of $MFe_{12}O_{19}$ is inversely proportional to the photoluminescence properties. At the same time, a similar phenomenon has been observed in Gd doped barium hexaferrite. [117, 118] Similar phenomena have been observed in other metal oxides and composites. [119-123]

6. CONCLUSIONS AND OUTLOOKS

$MFe_{12}O_{19}$-based photocatalysts have high magnetic properties, which makes its application in the field of photocatalysis has been unprecedented development. The recycling of $MFe_{12}O_{19}$-based photocatalysts by magnetic field can reduce the secondary pollution of photocatalyst to water. The photocatalytic activity of $MFe_{12}O_{19}$-based photocatalyst shows high synthesis method dependence, M ion dependence, dopant ion dependence and heterojunction dependence. The photocatalytic mechanism of $MFe_{12}O_{19}$-based photocatalyst is subject to the band arrangement theory like other photocatalysts. Simultaneously, due to the presence of Fe ions, part of the photocatalytic mechanism also follows the Z-scheme band arrangement theory. With the increase of photocatalytic activity, the fluorescence emission intensity of $MFe_{12}O_{19}$ decreased. Based on the current research trends, $MFe_{12}O_{19}$ photocatalyst can be developed in the following directions:

1. With the development of big data and intelligent artificial intelligence, it is of great research significance to simulate and predict the photocatalytic activity of $MFe_{12}O_{19}$ based on intelligent optimization algorithm to guide the experiment. This development trend is an effective way to save the cost of time, resources and manpower, and is conducive to making new breakthroughs and achievements. The performance prediction based on intelligence will be a mainstream direction in the synthesis of $MFe_{12}O_{19}$ photocatalyst in the future.

2. High entropy alloys have been demonstrated to have high photocatalytic activity, and coupling $MFe_{12}O_{19}$ with high entropy alloys may demonstrate higher photocatalytic activity for pollutant degradation. The photocatalytic mechanism of the coupling of the two is also a

hot topic. Since the photocatalytic mechanism of high entropy alloy itself is immature, the photocatalytic mechanism of high entropy alloy coupled with $MFe_{12}O_{19}$ photocatalyst is more complicated, but it is also a very worthy research topic.

3. The coupling between $MFe_{12}O_{19}$ photocatalyst and other metal-organic framework materials is also worth studying. Although a few literatures have reported the application of $MFe_{12}O_{19}$ coupled metal-organic framework materials in the field of photocatalysis, there are many kinds of metal-organic framework materials, and the photocatalytic activity after coupling with $MFe_{12}O_{19}$ photocatalysts is difficult to predict intuitively, so it is also a fruitful research topic.

4. When $MFe_{12}O_{19}$ is coupled with other types of luminescent materials, the mechanism of the intrinsic correlation between photocatalytic and luminescent properties may be different from the existing mechanism, which is also worthy of investigation. Meanwhile, combined with the study of upconversion luminescence, the photocatalytic mechanism and photoluminescence mechanism of $MFe_{12}O_{19}$ photocatalyst coupled with upconversion luminescence materials become more complicated and unclear.

5. $MFe_{12}O_{19}$-based photocatalyst has not been reported in any literature on photocatalytic hydrogen production from water and photocatalytic oxidation of heavy metal ions. Therefore, it is of great significance to design $MFe_{12}O_{19}$-based magnetic separation photocatalysts and study their applications in the decomposition of water to produce hydrogen and the oxidation of heavy metal ions. The calculation of the electronic state density of $MFe_{12}O_{19}$-based photocatalyst based on first principles will be helpful to the research and development of new $MFe_{12}O_{19}$-based photocatalysts.

COMPETING INTERESTS

The authors declare that they have no competing interests.

ACKNOWLEDGMENTS

This work was supported by the NSAF joint Foundation of China (U2030116), the Science and Technology Research Program of Chongqing Education Commission of China (KJZD-K202001202, KJQN202201204), the Chongqing Key Laboratory of Geological Environment Monitoring and Disaster Early-warning in Three Gorges Reservoir Area (No. ZD2020A0401), the Talent Introduction Project (09924601) of Chongqing Three Gorges University.

REFERENCES

[1] Xiang, Y.; Jiang, L.; Zhou, Y.; Luo, Z.; Zhi, D.; Yang, J.; Lam, S.S. Microplastics and environmental pollutants: key interaction and toxicology in aquatic and soil environments. Journal of Hazardous Materials 2022, 422, 126843. https://doi.org/10.1016/j.jhazmat.2021.126843

[2] Ramzan, M.; Iqbal, H.A.; Usman, M.; Ozturk, I. Environmental pollution and agricultural productivity in pakistan: new insights from ARDL and wavelet coherence approaches. Environmental Science and Pollution Research 2022, 29, 28749-28768. https://doi.org/10.1007/s11356-021-17850-3

[3] Cheng, T.; Gao, H.; Liu, G.; Pu, Z.; Wang, S.; Yi, Z.; Wu, X.; Yang, H. Preparation of core-shell heterojunction photocatalysts by coating CdS nanoparticles onto $Bi_4Ti_3O_{12}$ hierarchical microspheres and their photocatalytic removal of organic pollutants and Cr(VI) ion. Colloids and Surfaces A: Physicochemical and Engineering Aspects 2022, 633, 127918. https://doi.org/10.1016/j.colsurfa.2021.127918

[4] Yu, C.; Wang, S.; Zhang, K.; Li, M.; Gao, H.; Zhang, J.; Yang, H.; Hu, L.; Jagadeesha, A.V.; Li, D. Visible-light-enhanced photocatalytic activity of $BaTiO_3$/γ-Al_2O_3 composite photocatalysts for photodegradation of tetracycline hydrochloride. Optical Materials 2023, 135, 113364. https://doi.org/10.1016/j.optmat.2022.113364

[5] Saeed, M.; Muneer, M.; Akram, N. Photocatalysis: An effective tool for photodegradation of dyes—A review. Environmental Science and Pollution Research 2022, 29, 293-311. https://doi.org/10.1007/s11356-021-16389-7

[6] Li, L.; Gao, H.; Liu, G.; Wang, S.; Yi, Z.; Wu, X.; Yang. H. Synthesis of carnation flower-like $Bi_2O_2CO_3$ photocatalyst and its promising application for photoreduction of Cr(VI). Advanced Powder Technology 2022, 33, 103481. https://doi.org/10.1016/j.apt.2022.103481

[7] Wang, S.; Yu, C.; Chen, X.; Zhang, K.; Gao, H.; Yu, X.; Zhao, X.; Fang, L.; Cheng, X.; Zhang, J. Synthesis and characterization of $BaTiO_3/TiO_2$ heterojunction photocatalyst for novel application in photocatalytic degradation of TBBPA under simulated sunlight irradiation. ChemistrySelect 2022, 7, e202202764. https://doi.org/10.1002/slct.202202764

[8] Li, L.; Gao, H.; Yi, Z.; Wang, S.; Wu, X.; Li, R.; Yang. H. Comparative investigation on synthesis, morphological tailoring and photocatalytic activities of $Bi_2O_2CO_3$ nanostructures. Colloids and Surfaces A: Physicochemical and Engineering Aspects 2022, 644, 128758. https://doi.org/10.1016/j.colsurfa.2022.128758

[9] Li, L.; Sun, X.; Xian, T.; Gao, H.; Wang, S.; Yi, Z.; Wu, X.; Yang, H. Template-free synthesis of $Bi_2O_2CO_3$ hierarchical nanotubes self-assembled from ordered nanoplates for promising photocatalytic application. Physical Chemistry Chemical Physics 2022, 24, 8279–8295. https://doi.org/10.1039/D1CP05952A

[10] Wang, S.; Gao, H.; Jin, Y.; Chen, X.; Wang, F.; Yang, H.; Fang, L.; Chen, X.; Tang, S.; Li, D. Defect engineering in novel broad-band gap hexaaluminate $MAl_{12}O_{19}$ (M= Ca, Sr, Ba)-Based photocatalysts boosts near ultraviolet and visible

light-driven photocatalytic performance. Materials Today Chemistry 2022, 24, 100942. https://doi.org/10.1016/j.mtchem.2022.100942

[11] Gu, Y.; Guo, B.; Yi, Z.; Wu, X.; Zhang, J.; Yang, H. Morphology modulation of hollow-shell $ZnSn(OH)_6$ for enhanced photodegradation of methylene blue. Colloids and Surfaces A: Physicochemical and Engineering Aspects 2022, 653, 129908. https://doi.org/10.1016/j.colsurfa.2022.129908

[12] Han, M.; Wang, S.; Chen, X.; Liu, H.; Gao, H.; Zhao, X.; Wang, F.; Yang, H.; Yi, Z.; Fang, L. Spinel CuB_2O_4 (B= Fe, Cr, and Al) oxides for selective adsorption of Congo red and photocatalytic removal of antibiotics. ACS Applied Nano Materials 2022, 5, 11194-11207. https://doi.org/10.1021/acsanm.2c02349

[13] Cheng, T.; Gao, H.; Li, R.; Wang, S.; Yi, Z.; Yang, H. Flexoelectricity-induced enhancement in carrier separation and photocatalytic activity of a photocatalyst. Applied Surface Science 2021, 566, 150669. https://doi.org/10.1016/j.apsusc.2021.150669

[14] Wang, S.; Li, M.; Gao, H.; Yin, Z.; Chen, C.; Yang, H.; Fang, L.; Angadi, V.J.; Li, D. Construction of $CeO_2/YMnO_3$ and $CeO_2/MgA_{l2}O_4/YMnO_3$ photocatalysts and adsorption of dyes and photocatalytic oxidation of antibiotics: Performance prediction, degradation pathway and mechanism insight. Applied Surface Science 2023, 608, 154977. https://doi.org/10.1016/j.apsusc.2022.154977

[15] Pandiyan, R.; Dharmaraj, S.; Ayyaru, S.; Sugumaran, A.; Somasundaram, J.; Kazi, A.S.; Samiappan, S.C.; Ashokkumar, V.; Ngamcharussrivichai, C. Ameliorative photocatalytic dye degradation of hydrothermally synthesized bimetallic Ag-Sn hybrid nanocomposite treated upon domestic wastewater under visible light irradiation. Journal of Hazardous Materials 2022, 421, 126734. https://doi.org/10.1016/j.jhazmat.2021.126734

[16] Li, M.; Wang, S.; Gao, H.; Yin, Z.; Chen, C.; Yang, H.; Fang, L.; Veerabhadrappa, J.A.; Yi, Z.; Li, D. Selective removal of antibiotics over $MgA_{l2}O_4$/C3N4/$YMnO_3$ photocatalysts: Performance prediction and mechanism insight. Journal of the American Ceramic Society 2023. https://doi.org/10.1111/jace.18946

[17] Das, A.; Deka, T.; Kumar, P.M.; Bhagavathiachari, M.; Nair, R.G. Ag-modified ZnO nanorods and its dual application in visible light-driven photoelectrochemical water oxidation and photocatalytic dye degradation: A correlation between optical and electrochemical properties. Advanced Powder Technology 2022, 33, 103434. https://doi.org/10.1016/j.apt.2022.103434

[18] Wang, S.; Li, M.; Yin, Z.; Gao, H.; Liu, H.; Yang, H.; Fang, L.; Angadi, V.J.; Hu, L.; Li, D. Skillfully grafted C-O functional group to enhance the adsorption/photocatalytic mechanism of $YMnO_3/MgA_{l2}O_4$ heterojunction photocatalysts. Advanced Powder Technology 2022, 33, 103771. https://doi.org/10.1016/j.apt.2022.103771

[19] Singhal, S.; Namgyal, T.; Singh, J.; Chandra, K.; Bansal, S. A comparative study on the magnetic properties of $MFe_{12}O_{19}$ and $MAlFe_{11}O_{19}$ (M= Sr, Ba and Pb) hexaferrites with different morphologies. Ceramics International 2021, 37, 1833-1837. https://doi.org/10.1016/j.ceramint.2011.02.001

[20] Javadmoosavi, S.Y.; Naghizadeh, A.; Mizwari, Z.M.; Mortazavi-Derazkola, S. Biosynthesis of novel $NiFe_{12}O_{19}$-X (X= ZnO and TiO2) magnetic nanophotocatalyst toward the degradation pharmaceutical ceftriaxone sodium from aqueous solution under sunlight irradiation and antibacterial activity. Ceramics International 2023, 49, 1351-1361. https://doi.org/10.1016/j.ceramint.2022.09.116

[21] Naseri, K.; Khademi, E.; Mortazavi-Derazkola, S. Introducing a new pharmaceutical agent: Facile synthesis of $CuFe_{12}O_{19}$@ HAp-APTES magnetic nanocomposites and its cytotoxic effect on HEK-293 cell as an efficient *in vitro* drug delivery system for atenolol. Arabian Journal of Chemistry 2023, 16, 104404. https://doi.org/10.1016/j.arabjc.2022.104404

[22] Mahdiani, M.; Sobhani, A.; Salavati-Niasari, M. Enhancement of magnetic, electrochemical and photocatalytic properties of lead hexaferrites with coating graphene and CNT: Sol-gel auto-combustion synthesis by valine. Separation and Purification Technology 2017, 185, 140-148. https://doi.org/10.1016/j.seppur.2017.05.029

[23] Mahdiani, M.; Soofivand, F.; Salavati-Niasari, M. Investigation of experimental and instrumental parameters on properties of $PbFe_{12}O_{19}$ nanostructures prepared by sonochemical method. Ultrasonics Sonochemistry 2018, 40, 271-281. http://dx.doi.org/10.1016/j.ultsonch.2017.06.023

[24] Lahijani, B.; Hedayati, K.; Goodarzi, M. Magnetic $PbFe_{12}O_{19}$-TiO_2 nanocomposites and their photocatalytic performance in the removal of toxic pollutants. Main Group Metal Chemistry 2018, 41, 53-62. https://doi.org/10.1515/mgmc-2017-0055

[25] Asiabani, N.; Nabiyouni, G.; Khaghani, S.; Ghanbari, D. Green synthesis of magnetic and photo-catalyst $PbFe_{12}O_{19}$-PbS nanocomposites by lemon extract: nano-sphere $PbFe_{12}O_{19}$ and star-like PbS. Journal of Materials Science: Materials in Electronics 2017, 28, 1101-1114. https://doi.org/10.1007/s10854-016-5635-6

[26] Wang, S.; Gao, H.; Sun, G.; Zhang, J.; Xia, Y.; Xie, C.; Yang, G.; Wang, Y.; Fang, L. M-type barium hexaferrite nanoparticles synthesized by γ-ray irradiation assisted polyacrylamide gel method and its optical, magnetic and supercapacitive performances. Journal of Cluster Science 2021, 32, 569-578. https://doi.org/10.1007/s10876-020-01815-6

[27] Wang, S.; Gao, H.; Fang, L.; Hu, Q.; Sun, G.; Chen, X.; Yu, C.; Tang, S.; Yu, X.; Zhao, X. *et al*. Synthesis of novel $CQDs/CeO_2/SrFe_{12}O_{19}$ magnetic separation photocatalysts and synergic adsorption-photocatalytic degradation effect for methylene blue dye removal. Chemical Engineering Journal Advance 2021, 6, 100089. https://doi.org/10.1016/j.ceja.2021.100089

[28] Wang, S.; Chen, X.; Fang, L.; Gao, H.; Han, M.; Chen, X.; Xia, Y.; Xie, L.; Yang, H. Double heterojunction $CQDs/CeO_2/BaFe_{12}O_{19}$ magnetic separation photocatalysts: construction, structural characterization, dye and POPs removal, and the interrelationships between magnetism and photocatalysis. Nuclear Analysis 2022, 1, 100026. https://doi.org/10.1016/j.nucana.2022.100026

[29] Mahdiani, M.; Soofivand, F.; Ansari, F.; Salavati-Niasari, M. Grafting of $CuFe_{12}O_{19}$ nanoparticles on CNT and graphene: eco-friendly synthesis, characterization and photocatalytic activity. Journal of Cleaner Production 2018, 176, 1185-1197. https://doi.org/10.1016/j.jclepro.2017.11.177

[30] Chen, X.; Wang, S.; Gao, H.; Yang, H.; Fang, L.; Chen, X.; Tang, S.; Yu, C.; Li, D. A novel lead hexagonal ferrite ($PbFe_{12}O_{19}$) magnetic separation catalyst with excellent ultrasonic catalytic activity. Journal of Sol-Gel Science and Technology 2022, 1-16. https://doi.org/10.1007/s10971-022-05937-3

[31] Naceur, J.B.; Ayadi, F.; Cheikhrouhou-Koubaa, W.; Koubaa, M.; Nachbaur, V.; Chtourou, R.; Cheikhrouhou, A. Magnetic and Photocatalytic activity of pure $BaFe_{12}O_{19}$ and $BaFe_{12}O_{19}$-TiO_2 hexagonal ferrite nanocomposites. Journal of Superconductivity and Novel Magnetism 2022, 35, 3371-3378. https://doi.org/10.1007/s10948-022-06362-x

[32] Valero-Luna, C.; Palomares-Sanchéz, S.A.; Ruíz, F. Catalytic activity of the barium hexaferrite with H_2O_2/visible light irradiation for degradation of Methylene Blue. Catalysis Today 2016, 266, 110-119. http://dx.doi.org/10.1016/j.cattod.2015.08.049

[33] Bibi, I.; Majid, F.; Kamal, S.; Jilani, K.; Taj, B.; Nazeer, Z.; Iqbal, M. Enhanced visible light-driven photocatalytic degradation of crystal violet dye using Cr doped $BaFe_{12}O_{19}$ prepared via facile micro-emulsion route. Journal of Saudi Chemical Society 2022, 26, 101533. https://doi.org/10.1016/j.jscs.2022.101533

[34] Shawky, A.; Tashkandi, N.Y.; Albukhari, S.M.; Zaki, Z.I. $Ag_2O/BaFe_{12}O_{19}$ nanoheterojunctions for rapid photoelimination of atrazine herbicide in water under visible light. Ceramics International 2021, 47, 25721-25728. https://doi.org/10.1016/j.ceramint.2021.05.298

[35] Razavi, F.S.; Ghanbari, D.; Salavati-Niasari, M. Comparative study on the role of noble metal nanoparticles (Pt and Pd) on the photocatalytic performance of the $BaFe_{12}O_{19}/TiO_2$ magnetic nanocomposite: Green synthesis, characterization, and removal of organic dyes under visible light. Industrial & Engineering Chemistry Research 2022, 61, 13314-13327. https://doi.org/10.1021/acs.iecr.2c01066

[36] Zhang, T.; Zhou, P.; Zhang, L.; Xia, C.; Xie, M.; Guo, Q.; Chen, M.; Yuan, J.; Li, X.; Xu, Y. Construction lamellar $BaFe_{12}O_{19}/Bi_{3.64}Mo_{0.36}O_{6.55}$ photocatalyst for enhanced photocatalytic activity via a photo-Fenton-like Mo^{6+}/Mo^{4+} redox cycle. Chemosphere 2022, 307, 135909. https://doi.org/10.1016/j.chemosphere.2022.135909

[37] Xu, Y.; Ge, F.; Xie, M.; Huang, S.; Qian, J.; Wang, H.; He, M.; Xu, H.; Li, H. Fabrication of magnetic $BaFe_{12}O_{19}/Ag_3PO_4$ composites with an in situ photo-Fenton-like reaction for enhancing reactive oxygen species under visible light irradiation. Catalysis Science & Technology 2019, 9, 2563-2570. https://doi.org/10.1039/C8CY02449A

[38] Bahgat, M.; Khedr, M.H.; Abdel-Moaty, S.A. Reduction kinetics, photocatalytic activity and magnetic properties of $CoFe_2O_4/BaFe_{12}O_{19}$ core/shell nanoparticles. Materials Technology 2007, 22, 139-146. https://doi.org/10.1179/175355507X236641

[39] Feng, S.; Xie, T.; Kong, D.; Yang, F.; Li, T.; Yang, J.; Liu, M.; Du, H.; Su, Z. Boosting visible light photocatalysis in $BiOI/BaFe_{12}O_{19}$ magnetic heterojunction. Environmental Science and Pollution Research 2022, 1-13. https://doi.org/10.1007/s11356-022-24094-2

[40] Wang, H.; Xu, L.; Liu, C.; Jiang, Z.; Feng, Q.; Wu, T.; Wang, R. A novel magnetic photocatalyst $Bi_3O_4Cl/SrFe_{12}O_{19}$: Fabrication, characterization and its photocatalytic activity. Ceramics International 2020, 46, 460-467. https://doi.org/10.1016/j.ceramint.2019.08.283

[41] Xie, T.; Liu, C.; Xu, L.; Yang, J.; Zhou, W. Novel heterojunction $Bi_2O_3/SrFe_{12}O_{19}$ magnetic photocatalyst with highly enhanced photocatalytic activity. The Journal of Physical Chemistry C 2013, 117, 24601-24610. https://doi.org/10.1021/jp408627e

[42] Ghorbani, A.; Khalaji, A.D. β-$NaFeO_2$@ $SrFe_{12}O_{19}$ magnetic nanocomposite: synthesis, characterization, magnetic properties and antibacterial activity. Journal of Materials Science: Materials in Electronics 2022, 33, 7792-7798. https://doi.org/10.1007/s10854-022-07930-6

[43] Nourbakhsh, A.A.; Noorbakhsh, M.; Nourbakhsh, M.; Shaygan, M.; Mackenzie, K.J. The effect of nano sized $SrFe_{12}O_{19}$ additions on the magnetic properties of chromium-doped strontium-hexaferrite ceramics. Journal of Materials Science: Materials in Electronics 2011, 22, 1297-1302. https://doi.org/10.1007/s10854-011-0303-3

[44] Parkin, I.; Elwin, G.; Komarov, A.; Bui, Q.; Pankhurst, Q.; BarquÝn, L.; Morozov, Y. Convenient, low energy routes to hexagonal ferrites $MFe_{12}O_{19}$ (M= Sr, Ba) from SHS reactions of iron, iron oxide and MO_2 in air. Journal of Materials Chemistry 1998, 8, 573-578. https://doi.org/10.1039/A703774K

[45] Jean, M.; Nachbaur, V.; Bran, J.; Le Breton, J.M. Synthesis and characterization of $SrFe_{12}O_{19}$ powder obtained by hydrothermal process. Journal of Alloys and compounds 2010, 496, 306-312. https://doi.org/10.1016/j.jallcom.2010.02.002

[46] Mosleh, Z.; Kameli, P.; Ranjbar, M.; Salamati, H.J.C.I. Effect of annealing temperature on structural and magnetic properties of $BaFe_{12}O_{19}$ hexaferrite nanoparticles. Ceramics International 2014, 40, 7279-7284. https://doi.org/10.1016/j.ceramint.2013.12.068

[47] Almessiere, M.A.; Slimani, Y.; Trukhanov, A.V.; Sadaqat, A.; Korkmaz, A.D.; Algarou, N.A.; Aydin, H.; Baykal, A.; Toprak, M.S. Review on functional bi-component nanocomposites based on hard/soft ferrites: structural, magnetic, electrical and microwave absorption properties. Nano-Structures & Nano-Objects 2021, 26, 100728. https://doi.org/10.1016/j.nanoso.2021.100728

[48] Wang, S.F.; Chen, X.Y.; Gao, H.J.; Fang, L.M.; Hu, Q.W.; Sun, G.A.; Tang, S.; Liu, H.; Yu, C.; Pan, X.D. A comparative study on the phase structure, optical and NIR reflectivity of $BaFe_{12}O_{19}$ nano-pigments by the traditional and modified polyacrylamide gel method. Journal of Nano Research 2021, 67, 1-14. https://doi.org/10.4028/www.scientific.net/JNanoR.67.1

[49] Wang, S.; Li, D.; Xiao, Y.; Dang, W.; Feng, J. Synthesis of $SrFe_{12}O_{19}$ magnetic nanoparticles by EDTA complex method. Russian Journal of Physical Chemistry A 2017, 91, 1981-1986. https://doi.org/10.1134/S003602441710034X

[50] Wang, S.F.; Zhang, C.; Sun, G.; Chen, B.; Liu, W.; Xiang, X.; Wang, H.; Fang, L.; Tian, Q.; Ding, Q. *et al.* Effect of carbon and sintering temperature on the structural and magnetic properties of $SrFe_{12}O_{19}$ nanoparticles. Journal of Sol-Gel Science and Technology 2015, 73, 371-378. https://doi.org/10.1007/s10971-014-3543-x

[51] Bibi, F.; Iqbal, S.; Sabeeh, H.; Saleem, T.; Ahmad, B.; Nadeem, M.; Shakir, I.; PhD, M.A.; Kalsoom, A. Evaluation of structural, dielectric, magnetic and photocatalytic properties of Nd and Cu co-doped barium hexaferrite. Ceramics International 2021, 47, 30911-30921. https://doi.org/10.1016/j.ceramint.2021.07.274

[52] Bibi, I.; Muneer, M.; Iqbal, M.; Alwadai, N.; Almuqrin, A.H.; Altowyan, A.S.; Alshammari, F.H.; Almuslem, A.S.; Slimani, Y. Effect of doping on dielectric and optical properties of barium hexaferrite: Photocatalytic performance under solar light irradiation. Ceramics International 2021, 47, 31518-31526. https://doi.org/10.1016/j.ceramint.2021.08.030

[53] Muhiuddin, G.; Bibi, I.; Nazeer, Z.; Majid, F.; Kamal, S.; Kausar, A.; Raza, Q.; Alwasai, N.; Ezzine, S.; Iqbal, M. Synthesis of Ni doped barium hexaferrite by microemulsion route to enhance the visible light-driven photocatalytic degradation of crystal violet dye. Ceramics International 2022, 49, 4342–4355. https://doi.org/10.1016/j.ceramint.2022.09.319

[54] Nazeer, Z.; Bibi, I.; Majid, F.; Kamal, S.; Ibrahim, S.M.; Iqbal, M. Energy band gap tuning of $Ba_{1-x}Zn_xFe_{12-y}Cr_yO_{19}$ doped with Cr and Zn ions to enhance the optical, dielectric, ferroelectric, and photocatalytic properties. Optical Materials 2022, 125, 112090. https://doi.org/10.1016/j.optmat.2022.112090

[55] Khaliq, N.; Bibi, I.; Majid, F.; Sultan, M.; Amami, M.; Iqbal, M. Zn and Mn doped $Ba_{1-x}Zn_xFe_{12-y}Mn_yO_{19}$ as highly photoactive under visible light with enhanced electrochemical and dielectric properties. Materials Science in Semiconductor Processing 2022, 139, 106324. https://doi.org/10.1016/j.mssp.2021.106324

[56] Bibi, I.; Iqbal, S.; Majid, F.; Kamal, S.; Raza, Q.; Amami, M.; Katubi, K.M.; Alwadai, N.; Kareem, M.A.; Iqbal, M. The effect of Zn and Ni doping on the structural, optical, dielectric and photocatalytic properties of $Sr_{1-x}Zn_xFe_{1-y}Ni_yO_{19}$. Results in Physics 2022, 40, 105868. https://doi.org/10.1016/j.rinp.2022.105868

[57] Bibi, I.; Naz, T.; Majid, F.; Kamal, S.; Ata, S.; Almoneef, M.M.; Iqbal, S.; Iqbal, M. Band gap tuning of $BaFe_{12}O_{19}$ with Mg and Mn doping to enhance solar light absorption for photocatalytic application. International Journal of Energy Research 2021, 45, 11193-11205. https://doi.org/10.1002/er.6600

[58] Raza, Q.; Bibi, I.; Majid, F.; Kamal, S.; Ata, S.; Ghafoor, A.; Arshad, M.I.; Al-Mijalli, S.H.; Nazir, Arif.; Iqbal, M. Solar light-based photocatalytic removal of CV and RhB dyes using Bi and Al doped $SrFe_{12}O_{19}$ NPs and antibacterial properties. Journal of Industrial and Engineering Chemistry 2022, 118, 469-482 https://doi.org/10.1016/j.jiec.2022.11.030

[59] Ashraf, G.A.; Rasool, R.T.; Hassan, M.; Zhang, L. Enhanced photo Fenton-like activity by effective and stable Al–Sm M-hexaferrite heterogenous catalyst magnetically detachable for methylene blue degradation. Journal of alloys and compounds 2020, 821, 153410. https://doi.org/10.1016/j.jallcom.2019.153410

[60] Alonso-Rodríguez, D.W.; Ruiz-Luna, H.; Alfaro-Cruz, M.R.; Bañuelos-Frias, A.; Alvarado-Perea, L.; Valero-Luna, C. Synthesis and characterization of $BaFe_{12}O_{19}$-WC catalysts prepared by mechanical milling. Fuel 2020, 280, 118608. https://doi.org/10.1016/j.fuel.2020.118608

[61] Wang, H.; Xu, Y.; Jing, L.; Huang, S.; Zhao, Y.; He, M.; Xu, H.; Li, H. Novel magnetic $BaFe_{12}O_{19}$/g-C3N4 composites with enhanced thermocatalytic and photo-Fenton activity under visible-light. Journal of Alloys and Compounds 2017, 710, 510-518. https://doi.org/10.1016/j.jallcom.2017.03.144

[62] Xie, M.; Wang, D.; Jing, L.; Wei, W.; Xu, Y.; Xu, H.; Li, H.; Xie, J. Preparation of magnetically recoverable and Z-scheme $BaFe_{12}O_{19}$/AgBr composite for degradation of 2-Mercaptobenzothiazole and Methyl orange under visible light. Applied Surface Science 2020, 521, 146343. https://doi.org/10.1016/j.apsusc.2020.146343

[63] Mesdaghi, S.; Ghezelbash, S.; Yousefi, M. Structural, magnetic, and photocatalytic investigation of Hexaferrites/PANI nanocomposites. Materials Chemistry and Physics 2022, 281, 125866. https://doi.org/10.1016/j.matchemphys.2022.125866

[64] Xie, T.; Xu, L.; Liu, C.; Wang, Y. Magnetic composite $ZnFe_2O_4/SrFe_{12}O_{19}$: Preparation, characterization, and photocatalytic activity under visible light. Applied Surface Science 2013, 273, 684-691. https://doi.org/10.1016/j.apsusc.2013.02.113

[65] Wu, Q.; Yu, Z.; Wu, Y.; Gao, Z.; Xie, H. The magnetic and photocatalytic properties of nanocomposites $SrFe_{12}O_{19}/ZnFe_2O_4$. Journal of Magnetism and Magnetic Materials 2018, 465, 1-8. https://doi.org/10.1016/j.jmmm.2018.05.098

[66] Cui, C.; Xu, L.; Xie, T.; Peng, T. Synthesis and photocatalytic activity of magnetic heterostructure $ZnFe_2O_4$-$SrFe_{12}O_{19}$. Materials Technology 2016, 31, 454-462. https://doi.org/10.1080/10667857.2015.1105578

[67] Sobhani-Nasab, A.; Behpour, M.; Rahimi-Nasrabadi, M.; Ahmadi, F.; Pourmasoud, S. New method for synthesis of $BaFe_{12}O_{19}/Sm_2Ti_2O_7$ and $BaFe_{12}O_{19}/Sm_2Ti_2O_7$/Ag nano-hybrid and investigation of optical and photocatalytic properties. Journal of Materials Science: Materials in Electronics 2019, 30, 5854-5865. https://doi.org/10.1007/s10854-019-00883-3

[68] Ali, N.; Zada, A.; Zahid, M.; Ismail, A.; Rafiq, M.; Riaz, A.; Khan, A. Enhanced photodegradation of methylene blue with alkaline and transition-metal ferrite nanophotocatalysts under direct sun light irradiation. Journal of the Chinese Chemical Society 2019, 66, 402-408. https://doi.org/10.1002/jccs.201800213

[69] Polley, K.; Kundu, R.; Bera, J. Adsorption and sunlight-induced photocatalytic degradation of methyl blue by $BaFe_{12}O_{19}$ ferrite particles synthesised through co-precipitation method. International Journal of Environmental Analytical Chemistry 2021, 1-20. https://doi.org/10.1080/03067319.2021.1887165

[70] Mishra, D.D.; Tan, G. Visible photocatalytic degradation of methylene blue on magnetic $SrFe_{12}O_{19}$. Journal of Physics and Chemistry of Solids 2018, 123, 157-161. https://doi.org/10.1016/j.jpcs.2018.07.018

[71] Alimohammadi, E.; Sheibani, S.; Ataie, A. Preparation, magnetic and photocatalytic properties of nano-structured $SrFe_{12}O_{19}$ obtained via an optimized mechano-thermal route using celestite ore. Materials Chemistry and Physics 2022, 275, 125312. https://doi.org/10.1016/j.matchemphys.2021.125312

[72] Bavarsiha, F.; Montazeri-Pour, M.; Rajabi, M. Effect of non-aqueous media on nano-crystalline $SrFe_{12}O_{19}$ particles produced by co-precipitation with metal chlorides and evaluation of their magnetic and photocatalytic properties. Journal of Inorganic and Organometallic Polymers and Materials 2020, 30, 2386-2396. https://doi.org/10.1007/s10904-019-01414-7

[73] Gu, J.; Li, Q.; Long, X.; Zhou, X.; Liu, N.; Li, Z. Fabrication of magnetic dual Z-scheme heterojunction materials for efficient photocatalytic performance: The study of ternary novel MIL-88A (Fe)/BiOBr/$SrFe_{12}O_{19}$ nanocomposite. Separation and Purification Technology 2022, 289, 120778. https://doi.org/10.1016/j.seppur.2022.120778

[74] Yousefi, M.; Afghahi, S.S.S.; Amini, M.M.; Torbati, M.B. $Sr(CeNd)_xFe_{12-2x}O_{19}$/polythiophene nano-particles: Structral investigation, magnetic properties and photocatalyic activity. Inorganic Chemistry Communications 2020, 121, 108214. https://doi.org/10.1016/j.inoche.2020.108214

[75] Mishra, D.D.; Huang, Y.; Tan, G. Visible photocatalytic degradation of methylene blue on magnetic semiconducting La modified M-type Strontium Hexaferrite. arXiv 2017, 1712.04278. https://doi.org/10.48550/arXiv.1712.04278

[76] Bavarsiha, F.; Dadashian, S.; Montazeri-Pour, M.; Ghasemy-Piranloo, F.; Rajabi, M. Synthesis, characterization and photocatalytic efficiency of $Fe_3O_4/SiO_2/TiO_2$, $SrFe_{12}O_{19}/SiO_2/TiO_2$ and Fe_3O_4/SiO_2/ZnO core/shell/shell nanostructures. Processing and Application of Ceramics 2022, 16, 291-301. https://doi.org/10.2298/PAC2203291B

[77] Bavarsiha, F.; Rajabi, M.; Montazeri-Pour, M. Synthesis of $SrFe_{12}O_{19}/SiO_2/TiO_2$ composites with core/shell/shell nano-structure and evaluation of their photo-catalytic efficiency for degradation of methylene blue. Journal of Materials Science: Materials in Electronics 2018, 29, 1877-1887. https://doi.org/10.1007/s10854-017-8098-5

[78] Chenglun, L.; Hui, L.; Heping, Y.; Longjun, X. Preparation and visible-light-driven photocatalytic performance of magnetic $SrFe_{12}O_{19}/BiVO_4$. Journal of Materials Engineering and Performance 2015, 24, 771-777. https://doi.org/10.1007/s11665-014-1362-4

[79] Li, C.J.; Wang, J.N.; Li, X.Y.; Zhang, L.L. Functionalization of electrospun magnetically separable TiO_2-coated $SrFe_{12}O_{19}$ nanofibers: strongly effective photocatalyst and magnetic separation. Journal of materials science 2011, 46, 2058-2063. https://doi.org/10.1007/s10853-010-5038-7

[80] Liu, C.; Wang, Y.; Yang, J.; Xie, T.; Xu, L. Structure and catalytic activity of magnetic composite photocatalyst $SrFe_{12}O_{19}/SrTiO_3$. Materials Technology 2017, 32, 96-100. https://doi.org/10.1080/10667857.2015.1125629

[81] Xie, T.; Xu, L.; Liu, C.; Yang, J.; Wang, M. Magnetic composite BiOCl-$SrFe_{12}O_{19}$: a novel p-n type heterojunction with enhanced photocatalytic activity. Dalton Transactions 2014, 43, 2211-2220. https://doi.org/10.1039/C3DT52219A

[82] Xie, T.; Xu, L.; Liu, C.; Zhang, X. A novel magnetic heterojunction photocatalyst $TiO_2/SrFe_{12}O_{19}$: synthesis

strategy, photocatalytic activity, and unprecedented migration mechanism of photoexcited charge carrier. Materials Technology 2018, 33, 582-591.
https://doi.org/10.1080/10667857.2018.1483307

[83] Ebrahimi, Z.; Hedayati, K.; Ghanbari, D. Preparation of hard magnetic $BaFe_{12}O_{19}$-TiO_2 nanocomposites: applicable for photo-degradation of toxic pollutants. Journal of Materials Science: Materials in Electronics 2017, 28, 13956-13969.
https://doi.org/10.1007/s10854-017-7245-3

[84] Razavi, F.S.; Ghanbari, D.; Salavati-Niasari, M. Green synthesis of $SrFe_{12}O_{19}$@ Ag and $SrFe_{12}O_{19}$@ Au as magnetic plasmonic nanocomposites with high photocatalytic performance for degradation of organic pollutants. Chemosphere 2022, 291, 132741.
https://doi.org/10.1016/j.chemosphere.2021.132741

[85] Rezaei, A.; Nabiyouni, G.; Ghanbari, D. Photo-catalyst and magnetic investigation of $BaFe_{12}O_{19}$-ZnO nanoparticles and nanocomposites. Journal of Materials Science: Materials in Electronics 2016, 27, 11339-11352.
https://doi.org/10.1007/s10854-016-5258-y

[86] Karahroudi, Z.H.; Hedayati, K.; Goodarzi, M. Green synthesis and characterization of hexaferrite strontium-perovskite strontium photocatalyst nanocomposites. Main group metal chemistry 2020, 43, 26-42.
https://doi.org/10.1515/mgmc-2020-0004

[87] Mohanta, O.; Singhbabu, Y.N.; Giri, S.K.; Dadhich, D.; Das, N.N.; Sahu, R.K. Degradation of Congo red pollutants using microwave derived $SrFe_{12}O_{19}$: an efficient magnetic photocatalyst under visible light. Journal of alloys and compounds 2013, 564, 78-83.
https://doi.org/10.1016/j.jallcom.2013.02.074

[88] Rasheed, A.; Bibi, I.; Majid, F.; Kamal, S.; Taj, B.; Raza, M.A.S.; Khaliq, N.; Katubi, K.M.; Ezzine, S.; Alwadai, N. *et al*. Mn doped $SrFe_{12}O_{19}$ fabricated via facile microemulsion route and solar-light-driven photocatalytic removal of crystal violet dye. Physica B: Condensed Matter 2022, 646, 414303.
https://doi.org/10.1016/j.physb.2022.414303

[89] Irshad, Z.; Bibi, I.; Ghafoor, A.; Majid, F.; Kamal, S.; Ezzine, S.; Elqahtani, Z.M.; Alwadai, N.; Messaoudi, N.E.; Iqbal, M. Ni doped $SrFe_{12}O_{19}$ nanoparticles synthesized via micro-emulsion route and photocatalytic activity evaluation for the degradation of crystal violet under visible light irradiation. Results in Physics 2022, 42, 106006.
https://doi.org/10.1016/j.rinp.2022.106006

[90] Kaur, P.; Kaushik, A.; Singhal, S. Comparative evaluation of photocatalytic performance of hexagonal ferrites procured via sol-gel route. Materials Today: Proceedings 2019, 14, 426-434.
https://doi.org/10.1016/j.matpr.2019.04.165

[91] Mohammadi, K.; Sadeghi, M.; Azimirad, R.; Ebrahimi, M. Barium Hexaferrite nanoparticles: Morphology-controlled preparation, characterization and investigation of magnetic and photocatalytic properties. Journal of Materials Science: Materials in Electronics 2017, 28, 9983-9988.
https://doi.org/10.1007/s10854-017-6747-3

[92] Chen, S.; Di, Y.; Li, H.; Wang, M.; Jia, B.; Xu, R.; Liu, X. Efficient photocatalytic dye degradation by flowerlike MoS_2/$SrFe_{12}O_{19}$ heterojunction under visible light. Applied Surface Science 2021, 559, 149855.
https://doi.org/10.1016/j.apsusc.2021.149855

[93] Mohammadi, K.; Sadeghi, M.; Azimirad, R. Facile synthesis of $SrFe_{12}O_{19}$ nanoparticles and its photocatalyst application. Journal of Materials Science: Materials in Electronics 2017, 28, 10042-10047.
https://doi.org/10.1007/s10854-017-6763-3

[94] Farghali, A.A.; Khedr, M.H.; Moustafa, A.F. Photocatalytic activity and magnetic properties of nanocrystallite strontium hexaferrite prepared by self-flash combustion. Materials Technology 2008, 23, 104-109.
https://doi.org/10.1179/175355508X310089

[95] Fu, W.; Yang, H.; Li, M.; Chang, L.; Yu, Q.; Xu, J.; Zou, G. Preparation and photocatalytic characteristics of core-shell structure TiO_2/$BaFe_{12}O_{19}$ nanoparticles. Materials Letters 2006, 60, 2723-2727.
https://doi.org/10.1016/j.matlet.2006.01.078

[96] Brahimi, B.; Mekatel, E.; Mellal, M.; Trari, M. Synthesis of the hexaferrite semiconductor $SrFe_{12}O_{19}$ and its application in the photodegradation of Basic Red 46. Journal of Materials Science: Materials in Electronics 2021, 32, 17780-17790.
https://doi.org/10.1007/s10854-021-06314-6

[97] Xu, X.; Song, W. A new application field for $BaFe_{12}O_{19}$ used as visible light photocatalyst. Materials Technology 2020, 35, 395-401.
https://doi.org/10.1080/10667857.2019.1688538

[98] Zhang, T.; Qing, D.; Jiang, Z.; Xu, L.; Liu, C.; Yang, Z.; Huang, G. Reduced graphene oxide modified $BiOC_l$/Co-doped$SrFe_{12}O_{19}$ composite for photocatalytic degradation of Rhodamine B. Optical Materials 2022, 129, 112547.
https://doi.org/10.1016/j.optmat.2022.112547

[99] Wang, H.; Xu, L.; Wu, X.; Zhang, M. Eco-friendly synthesis of a novel magnetic $Bi_4O_5Br_2$/$SrFe_{12}O_{19}$ nanocomposite with excellent photocatalytic activity and recyclable performance. Ceramics International 2021, 47, 8300-8307.
https://doi.org/10.1016/j.ceramint.2020.11.191

[100] Jiang, Z.; Zou, Y.; Hao, Y.; Xu, L.; Liu, C.; Su, H.; Gong, S. Magnetic recyclable ZnO/$SrFe_{12}O_{19}$ photocatalyst for effective photodegradation of rhodamine B under simulated sunlight. International Journal of Hydrogen Energy 2022, 47, 34387-34396.
https://doi.org/10.1016/j.ijhydene.2022.08.038

[101] Jiang, Z.; Yin, X.; Hao, Y.; Xu, L.; Liu, C.; Feng, Q. Novel magnetic composite photocatalyst ZnO/$Bi_{24}O_{31}Br_{10}$@ $SrFe_{12}O_{19}$ with enhanced photocatalytic activity. aterials Technology 2022, 37, 324-331.
https://doi.org/10.1080/10667857.2020.1837543

[102] Bibi, I.; Iqbal, S.; Majid, F.; Fatima, N.; Alwadai, N.; Iqbal, M. Solar-light-driven photocatalytic performance of Cr and Co doped $Sr_{1-x}Co_xFe_{12-y}Cr_yO_{19}$ and effect of doping on optical, structural and dielectric properties. Optical Materials 2022, 124, 111961.
https://doi.org/10.1016/j.optmat.2021.111961

[103] Xie, T.; Hu, J.; Yang, J.; Liu, C.; Xu, L.; Wang, J.; Peng, Y.; Liu, S.; Yin, X.; Lu, Y. Visible-light-driven photocatalytic activity of magnetic BiOBr/$SrFe_{12}O_{19}$ nanosheets. Nanomaterials 2019, 9, 735.
https://doi.org/10.3390/nano9050735

[104] Qing, D.; Xie, T.; Yang, J.; Liu, C.; Xu, L. A novel nano-magnetic heterostructure $BiOC_l$/Co-doped $SrFe_{12}O_{19}$: synthesis and photocatalytic activity. Materials Technology 2019, 34, 652-664.
https://doi.org/10.1080/10667857.2019.1612550

[105] Kaur, P.; Singh, S.; Aggarwal, D.; Kumar, V.; Tikoo, K.; Kaushik, A.; Singhal, S. Synergizing hexagonal ferrite with transition metals in core-shell-shell nanostructures (SrFe@ Dop@ M) as dualistic probe for detoxification and electrochemical detection of pharmaceutical drugs. Ceramics International 2022.
https://doi.org/10.1016/j.ceramint.2022.10.111

[106] Raut, S.S.; Adpa, S.K.; Jambhale, A.; Abhyankar, A.C.; Kulkarni, P.S. Enhanced photocatalytic activity of magnetic $BaFe_{12}O_{19}$ nanoplatelets than TiO_2 with emphasis on reaction kinetics, mechanism, and reusability. Industrial & Engineering Chemistry Research 2018, 57, 16192-16200.
https://doi.org/10.1021/acs.iecr.8b02859

[107] Ramezanalizadeh, H.; Rafiee, E. Very fast photodegradation of tetracycline by a novel ternary nanocomposite as a visible light driven photocatalyst. Materials Chemistry and Physics 2021, 261, 124242.
https://doi.org/10.1016/j.matchemphys.2021.124242

[108] Abd Aziz, A.; Ibrahim, S.; Saravanan, P. Nanocrystal TiO_2 engulfed SiO_2-barium hexaferrite for enhanced electrons

mobility and solar harvesting potential. Materials Science Forum 2015, 819, 226-231.
https://doi.org/10.4028/www.scientific.net/MSF.819.226

[109] Abd Aziz, A.; Yau, Y.H.; Puma, G.L.; Fischer, C.; Ibrahim, S.; Pichiah, S. Highly efficient magnetically separable TiO_2–graphene oxide supported $SrFe_{12}O_{19}$ for direct sunlight-driven photoactivity. Chemical Engineering Journal 2014, 235, 264-274.
https://doi.org/10.1016/j.cej.2013.09.043

[110] Ma, J.; Hong, Y.; Sun, Y.; Peng, F. Fabrication of CeO_2 microspheres by sol− gel reaction with polymerization via single emulsion. Nuclear Analysis 2022, 1, 100008.
https://doi.org/10.1016/j.nucana.2022.100008

[111] Fang, L.; Chen, X.; Xie, L.; Sun, G.; Chen, B.; Peng, S. The neutron diffraction experiments under high pressure and high temperature on FENGHUANG diffractometer at CMRR. Nuclear Analysis 2022, 1, 100023.
https://doi.org/10.1016/j.nucana.2022.100023

[112] Anantharamaiah, P.N.; Chandra, N.S.; Shashanka, H.M.; Kumar, R.; Sahoo, B. Magnetic and catalytic properties of Cu-substituted $SrFe_{12}O_{19}$ synthesized by tartrate-gel method. Advanced Powder Technology 2020, 31, 2385-2393.
https://doi.org/10.1016/j.apt.2020.04.004

[113] Abdel-Latif, I.A.; Singh, C.; Joshi, R.; Singh, J.; Gismelssed, A.; Alam, M.M.; Al-Hajji, L.A.; Faisal, M.; Asiri, A.M. *et al.* Fabrication of highly sensitive 4-Nitrophenol sensor and photocatalytic performance of multifunctional $Ba_{0.5}Sr_{0.5}Co_xHf_xFe_{12-2x}O_{19}$ Ferrite. Materials Chemistry and Physics 2022, 288, 126396.
https://doi.org/10.1016/j.matchemphys.2022.126396

[114] Brightlin, B.C.; Balamurugan, S.; Arun, T. Microstructural and magnetic features of $SrFe_{12}O_{19}$ materials synthesized from different fuels by Sol-Gel auto-combustion method. Journal of Superconductivity and Novel Magnetism 2017, 30, 1427-1437.
https://doi.org/10.1007/s10948-016-3940-1

[115] Khan, I.S.; Gul, I.H. Comparative investigation of magnetic, di-electric, optical, and electrical properties of mono-$BaFe_2O_4$ and hexa-$BaFe_{12}O_{19}$ nano-ferrites for photovoltaic (PV) applications. Applied Physics A 2022, 128, 1-16.
https://doi.org/10.1007/s00339-022-06214-4

[116] Balamurugan, S.; Brightlin, B.C.; Jainshaa, J. Physical properties of $BaFe_{12}O_{19}$ materials obtained under different pH using hexamine as novel fuel by auto combustion followed by annealing route. Journal of Nanoscience and Nanotechnology 2020, 20, 87-95.
https://doi.org/10.1166/jnn.2020.16888

[117] Mahapatro, J.; Agrawal, S. Optical, dielectric and electrical properties of Gd3+ ions doped barium hexaferrite ceramic compounds for microwave device applications. Journal of Alloys and Compounds 2022, 907, 164405.
https://doi.org/10.1016/j.jallcom.2022.164405

[118] Mahapatro, J.; Agrawal, S. Photoluminescence behaviour of Gd doped barium hexaferrite. In IOP Conference Series: Materials Science and Engineering 2020, 798, 012011.
https://doi.org/10.1088/1757-899X/798/1/012011

[119] Gao, H.; Wang, S.; Wang, Y.; Yang, H.; Fang, L.; Chen, X.; Yi, Z.; Li, D. Fabrication and characterization of $BaMoO_4$-Coupled $CaWO_4$ heterojunction micro/nanocomposites with enhanced photocatalytic activity towards MB and CIP degradation. Journal of Electronic Materials 2022, 51, 5230-5245.
https://doi.org/10.1007/s11664-022-09769-3

[120] Gao, H.; Wang, Y.; Wang, S.; Yang, H.; Yi, Z. A simple fabrication, microstructure, optical, photoluminescence and supercapacitive performances of $MgMoO_4/MgWO_4$ heterojunction micro/nanocomposites. Solid State Sciences 2022, 106909.
https://doi.org/10.1016/j.solidstatesciences.2022.106909

[121] Gao, H.; Wang, S.; Wang, Y.; Yang, H.; Wang, F.; Tang, S.; Yi, Z.; Li, D. $CaMoO_4/CaWO_4$ heterojunction micro/nanocomposites with interface defects for enhanced photocatalytic activity. Colloids and Surfaces A: Physicochemical and Engineering Aspects 2022, 642, 128642.
https://doi.org/10.1016/j.colsurfa.2022.128642

[122] Gao, H.; Yu, C.; Wang, Y.; Wang, S.; Yang, H.; Wang, F.; Tang, S.; Yi, Z.; Li, D. A novel photoluminescence phenomenon in a $SrMoO_4/SrWO_4$ micro/nano heterojunction phosphors obtained by the polyacrylamide gel method combined with low temperature calcination technology. Journal of Luminescence 2022, 243, 118660.
https://doi.org/10.1016/j.jlumin.2021.118660

[123] Wang, Y.; Gao, H.; Wang, S.; Fang, L.; Chen, X.; Yu, C.; Tang, N.; Liu, H.; Yi, Z.; Yang, H. Facile synthesis of $BaMoO_4$ and $BaMoO_4/BaWO_4$ heterostructures with type-I band arrangement and enhanced photoluminescence properties. Advanced Powder Technology 2021, 32, 4186-4197.
https://doi.org/10.1016/j.apt.2021.09.028

Received on 06-12-2022 Accepted on 28-12-2022 Published on 31-12-2022

DOI: https://doi.org/10.12974/2311-8741.2022.10.06